Development of Infrared Evanescent Wave Fibre Sensors using an FTIR Spectrometer

By

Kieran O'Dwyer B.Sc.

Supervised by

Dr. Vincent Ruddy

Department of Physical Sciences

Dublin City University

Ireland

M.Sc. **September 1993**

Development of Infrared Evanescent Wave Fibre Sensors using an FTIR Spectrometer

By

Kieran O'Dwyer B.Sc.

A Thesis Presented

to

Dublin City University

for the

Degree of Master of Science

Supervised by

Dr. Vincent Ruddy

Department of Physical Sciences

Dublin City University

Ireland

September 1993

Declaration

I hearby certify that this material, which I now submit for assessment on the program of study leading to the award of Master of Science is entirely my own work and has not been taken from the work of others save and to the extent that such work has been cited and acknowledged within the text of my work.

Signed: Kieran O'Dwyer

Kieran O'Dwyer

Date: 9/11/93

Acknowledgements

I would like to thank anyone who helped in any way towards the completion of this project. In particular, I wish to thank my supervisor Dr. Vincent Ruddy for his untiring help and encouragement and Dr. Brian MacCraith for his advice and direction during the course of this work.

I would like to thank Simon and Dave, the other members of the infrared trio, for their help and comradeship in confined spaces and also all the members of the optical sensors group, Fergal, Jude, Kieran, Ger, Tom, Dave and Clarke for two great years.

To all the post-graduate students in the physics department and also the physics technicians especially Des and Cian in the workshop for services beyond the call of duty.

To "Le Verre Fluore" and "Culham Laboratries" for the provision of equipment and support for this project.

Finally, but not in order of importance, I would like to thank my parents for their support and understanding and to Janet for her encouragement during the course of this work.

Dedication

I would like to dedicate this masters to Janet, for all the encouragement during the last three years and to Mum and Dad for persevering with me when it looked like I would never leave college.

Abstract

The detection of gases via their absorption bands in the mid infrared portion of the spectrum is discussed. Various fibre optic probe designs suitable for use with Fourier Transform Infrared (FTIR) spectrometers are described. The probes fabrication and evaluation with various gases, hydrocarbons and flue gas products are described. Porous clad fibres, tapered fibres, special capillary type fibres and fibre fed transmission cells are all used and their minimum detection concentration (MDC) values quoted for various gases. Evanescent wave absorption spectroscopy of relevance to both the porous clad and tapered fibre probes is compared to the direct transmission cell spectroscopy in terms of sensitivity. The poor sensitivity of the tapered fibre probe is attributed to the underfilled local numerical aperture in the sensing region. The potential of evanescent wave fibre probes coupled to FTIR spectrometers is discussed in the context of both inflammable gas detection and flue gas analysis. Experimental detection limits of various gases are reported and compared to model predictions.

List of Figures

List of Tables

Table of Contents

CHAPTER 1

Chapter 1
Introduction

1.1 Mid Infrared Spectroscopy

The detection of chemical species via absorption or emission lines or bands is an analytical tool commonly carried out using an absorption or emission spectrometer. The wavelength of the spectral structure is used to identify the constituents of the sample and the extent of the absorption or emission to quantify the concentration of each component. In the case of absorption spectroscopy the absorbance of the sample scales linearly with concentration in accordance with the Lambert Beer Law where the measurement is made at an analytical wavelength of the chemical. The location of the analytical wavelength is determined by the energy levels which give rise to the absorption or emission transmission.

In the case of molecules, vibrational and rotational energy levels are typically in the infrared portion of the spectrum with the photon energies for transitions among rotational levels being very small and falling in the far infrared region. The availability of infrared transmitting fibres has opened up both the so called "fingerprint" and "overtone" regions of the spectrum to remote spectroscopy. The transmission of mid infrared radiation to and from a Fourier Transform Spectrometer using special IR transmitting fibres will be discussed in this thesis together with techniques of enhancing detection sensitivity using fibre tapering, transmission cells and special capillary fibres. The technique of MIR (mid infrared) spectroscopy is well established. This work reports on remote MIR spectroscopy using MIR transmitting fibres to take the signal to and from a sensing zone using the IR source and detector system of a Fourier Transform Infrared Spectrometer.

1.2 Fluoride Fibre

Conventional telecommunication silica fibre becomes highly attenuating at wavelengths in excess of about 1.5μm as shown in Van Etten and Van Der Plaats (1991). The infrared tail in the transmittance curve makes such fibre unsuitable for transmission of radiation in the mid IR portion of the spectrum. Three families of glasses have been developed with low attenuations in the infrared: fluoride, chalcogenide and silver halide. In this work fluoride fibre manufactured by "Le Verre Fluore" France was used. As can be seen from Table 1.1 (the manufacturers specifications) the attenuation of this Zirconium Fluoride glass is less than 1dB/m in the 1-4μm wavelength region of the infrared spectrum (3dB/m refers to an attenuation of approximately 50% of the optical power over a 1m length of fibre). Since the publication of this specification lower attenuation figures have been achieved particularly in the 2-3μm region of the spectrum. British Telecom reported in 1990 the achievement of a loss of 0.65 dB/km at a wavelength of 2.59μm with fluoride glass fibre (Carter et al. 1990). This multimode step index fibre has a numerical aperture of 0.2 and is coated with UV cured polyacrylate. Attenuations of these orders of magnitude permit the transmission of appreciable quantities of optical power to and from sensing zones located up to some 100m from a spectrometer.

Table 1.1 Infrared Fibre Optic Cables from "Le Verre Fluore"

Fibre structure	Step index
Core and cladding material	Zirconium fluoride glasses
Coating material	UV cured polyacrylate
Attenuation between 0.5 & 4.2μm	< 1dB/m
Numerical aperature	0.2
Standard core/cladding diameters (μm)	70/140 150/200 200/250 350/400 450/500 1000/1200
Standard connectors	Cylindrical -diameter/length: 3.5/25mm (REF CC), SMA (REF CS)

1.3 Evanescent Wave Sensing

The ray treatment of total internal reflection predicts no electromagnetic radiation in the lower index medium for light incident at the interface at angles greater than the critical angle θ_c given by $Sin^{-1}\, n_2/n_1$ (n_1 and n_2 being the refractive indices of the higher and lower index media respectively). Wave theory however predicts the

existence in the lower refractive index medium of a wave which

i) propagates in the direction of the interface

ii) decays exponentially in amplitude with distance from the interface - see Figure 1.1 Egalon (1990).

Figure 1.1 Bound mode (ray) and its evanescent counterpart in an optical fibre

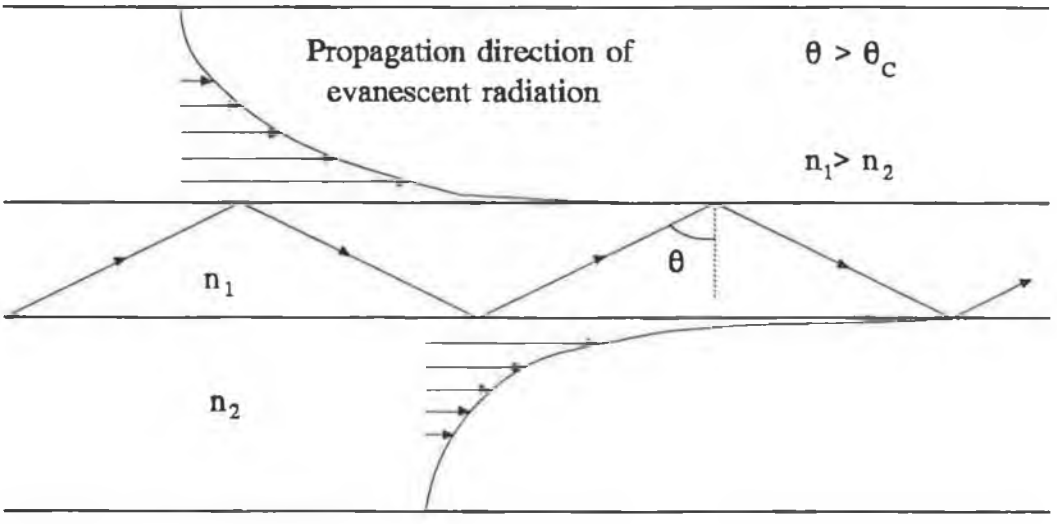

When the lower index medium is purely refractive (ie the refractive index has a real component and no imaginary or absorption related component) the optical power associated with this so called evanescent wave oscillates periodically between the two media. When however the lower index medium is absorbing (at the wavelength of the radiation being used) on its excursion into the medium some optical power is absorbed and as a result the total transmitted power is partially absorbed and so the total transmitted power in the higher index (n_1) medium is reduced. This effect is known as frustrated total internal reflection and is the basis of evanescent wave spectroscopy or internal reflection spectroscopy as referred to by Harrick (1987).

At a planar interface the electric field decays exponentially with distance from the interface with a 1/e depth of

$$\frac{\lambda}{2\pi n_1\sqrt{Sin^2\theta - (n_2/n_1)^2}} \qquad \text{Eqn 1.1}$$

where θ is the angle made by the ray to the normal at the interface. Thus for rays close to the critical angle substantial E field penetration occurs in the lower index

medium and as a result strong absorption occurs if the medium is absorbing at the wavelength of light used (λ is the free space or vacuum wavelength of the light).

In the cylindrical optical waveguide such as a step index fibre total internal reflection is the mechanism by which light propagates as bound modes. Solutions of the wave equation in cylindrical polar co-ordinates involve core and cladding parameters U and W which are given by

$$U = a\sqrt{n_1^2k^2 - \beta^2} \qquad \text{Eqn 1.2}$$

$$W = a\sqrt{\beta^2 - n_2^2k^2}$$

- see Synder and Love (1983).

For a fibre of core radius a and radiation of wavenumber k ($= 2\pi/\lambda$), β is the propagation constant of a particular ray or mode and is given by the component of the wavevector n_1k along the core axis ie. $n_1k\ Cos\theta_z$.

Figure 1.2 Propagation orientation

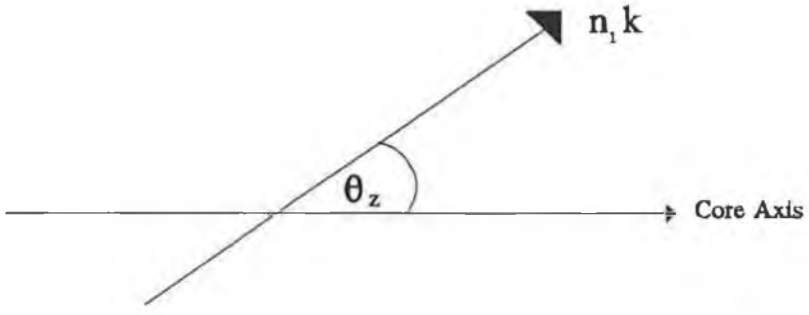

U and W are related to the normalised frequency or V number of the fibre by

$$V^2 = U^2 + W^2 \qquad \text{Eqn 1.3}$$

The evanescent wave in the cladding can be represented by (Synder and Love 1983, Eqn 12-12)

$$K_l\left(W\frac{r}{a}\right) \qquad \text{Eqn 1.4}$$

where K_l is the modified Bessel function of order l and r is the distance from the core axis. Provided r is not close to the value a the K_l function is approximately an exponential (Abramowitz and Stegun (1964), Figure 9.7) and so the evanescent E field are approximately exponential with a 1/e depth of

$$\frac{a}{W} \qquad \text{Eqn 1.5}$$

which agrees with Eqn 1.1 for the plane waveguide case. It should be noted that in fibre waveguide theory angles θ are usually measured with respect to the fibre axis and so are the complements of the planar waveguide angles ie

$$\theta_{W.G.} \rightarrow \frac{\pi}{2} - \theta_{Pl.} \qquad \text{Eqn 1.6}$$

When a mode is close to cut off or $W \rightarrow 0$ the evanescent wave penetration depth is large.

The number of bound modes a fibre can carry is given by

$$N \simeq \frac{V^2}{2} \qquad \text{Eqn 1.7}$$

and the fractional optical power in the lower index or cladding region is

$$f \simeq \frac{4}{3\sqrt{N}} \simeq \frac{4\sqrt{2}}{3V} \qquad \text{Eqn 1.8}$$

as shown by Gloge (1971)

Thus in evanescent wave spectroscopy using an optical fibre as the waveguide, sensitivity depends on $1/V$ and is larger for small diameter core fibres[1].

[1] V is defined by $2\pi a(n_1^2-n_2^2)^{1/2}/\lambda$

Just as in transmission cell spectroscopy optical power reduces exponentially with propagation distance z in the case of a fibre with the absorbance A being directly proportional to the product

$$f\varepsilon bc \qquad \text{Eqn 1.9}$$

where f is the fraction of power in the cladding

ε is the absorptivity of the absorbing chemical

b is the length of the fibre cladding immersed in the chemical

and c is the concentration of the chemical

or stated differently the attenuation coefficient for evanescent wave sensing scales linearly with f and α where α is the bulk attenuation coefficient (for direct transmission spectroscopy) and is given by εc.

The detection of a chemical using a fibre evanescent wave probe thus involves the evanescent wave of the propagating modes in the fibre gaining access to the chemical. This can occur if the fibre cladding is partly or fully removed in the sensing region or if the natural cladding material is permeable to the species to be detected. Several examples of unclad IR transmitting fibres being used for evanescent wave spectroscopy have been reported Margalit et al (1989), Katz et al (1991), Driver et al (1991), Messica et al (1991) and Heo et al (1991).

An example of permeable claddings are polymer clad fibres such as polymethyl methacrylate (PMMA) and polytetrafluoroethylene (PTFE) clad fluoride core fibres and sol-gel glass cladding fibres. The former are commercially available, the latter are fabricated in laboratories for localised sensing. Polymer clad fibres used as sensors have been reported by Krska et al (1992) and Ruddy et al (1990b) and (1993a), while sol-gel coated (ie clad) fibres have been used as sensors as reported by Mac Craith et al (1991b).

1.4 Fibre Probe Configurations

In the detection of chemical species using evanescent wave fibre probes in conjunction with a spectrophotometer there are a number of possible designs. The

Figure 1.3 Polished fibre

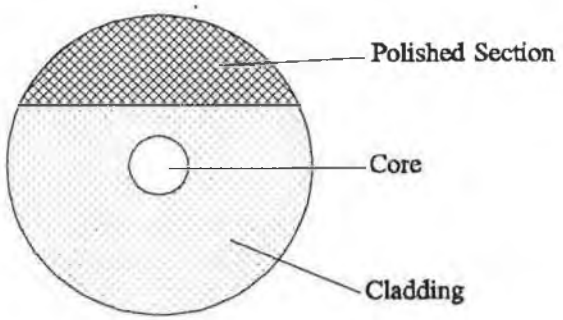

fibre may be polished to access parts of the cladding region to form a D shape configuration as discussed by Muhammad and Steward (1992) and Tseng and Chen (1992). This configuration maintains mechanical strength of the fibre as much of the primary coating and cladding is retained. An equivalent approach is the use of an eccentrically cladded fibre as discussed by Yoshikawa et al (1988).

Figure 1.4 Eccentrically clad fibre

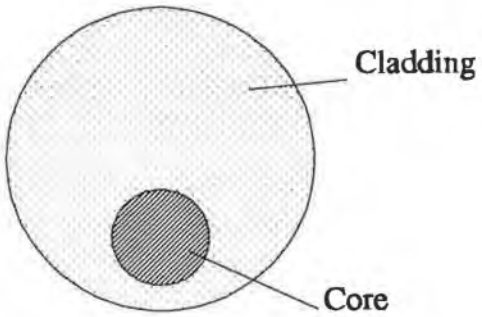

Where polymer clad fibre is available the cladding may be removed chemically in a sensing zone, cleaned and then used to expose the evanescent fields of the guided core modes to the absorbing chemical. The overall effect of the removal of both primary coating and cladding in a particular sensing region of the fibre leads to a very brittle device which is easily broken. The weakly guiding fibre (core and cladding refractive indices are very close in magnitude) becomes in the sensing region a strongly guiding one unless the refractive index of the species being absorbed is close to that of the glass or polymer cladding it has replaced. If the sensing zone is "strongly guiding" the fraction of optical power outside the core is reduced even further from the $1/V_{fibre}$ value (approx.) from Eqn 1.8. Refractive index uncertainties or variations in the fibre will also cause uncertainties in interpretation of power

attenuation measurements as mode stripping and evanescent wave attenuation will both give rise to the same effect.

Fibre tapering is another approach to fibre sensing. When the core diameter is reduced (by fibre elongation at a taper) the effective V number of the fibre is reduced (since V depends linearly on core radius a) and as a result the evanescent power fraction f (proportional to $1/V$) increases for the taper region.

Figure 1.5 Fibre taper

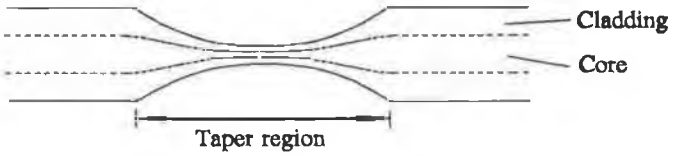

The increased evanescent power fraction f causes a similar increase in absorbance A. Like their counterpart the bare unclad core tapers may also be very brittle and easily broken.

Hollow glass fibres which behave as waveguides because of anomalous dispersion of the glass in a certain wavelength band have been reported. These have been used by Saito et al (1992) to detect the presence of various pollution gases such as NO_x, SO_2 and hydrocarbons. The fibre core (in this case the hollow centre of the waveguide) acts as the sample cell ie. the sensor is a transmission cell rather than evanescent wave device. Worrell et al (1992) report such a device used in the detection of ethylene gas at the ppm level.

Figure 1.6 Hollow glass fibre

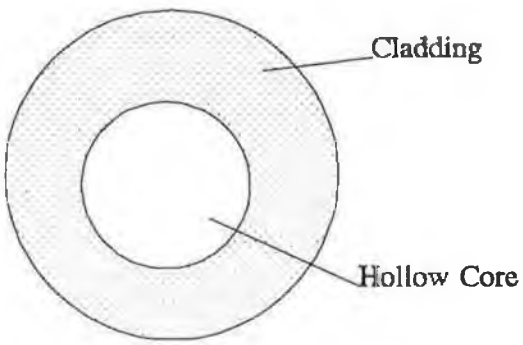

Porous clad fibre sensors in which a gas or liquid diffuses into the cladding material pores where it can absorb the evanescent waves of the propagating modes are the least invasive of all evanescent wave sensors and the inherent mechanical stability of the fibre is not reduced. In addition the effective index of the cladding material is not substantially modified by the presence of a gas in the pores and so the fibre does not change from weakly guiding to strongly guiding in the sensing region, resulting in no loss of detection sensitivity as discussed earlier. Gas diffusion rates into the cladding limit the response time of such a sensor.

Finally an evanescent sensor consisting of a glass core supported within a hollow glass capillary as shown below may be considered.

Figure 1.7 Novel sensing fibre

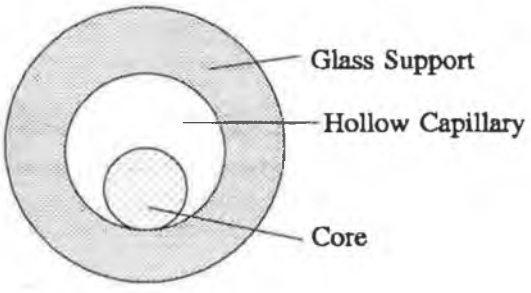

Fluids present within the hollow capillary will interact with the evanescent fields of the light propagating in the core. This design is attractive for gas detection. This capillary type fibre is specially fabricated for sensing purposes.

A fibre may of course be used to transmit infrared radiation to and from a transmission cell containing the absorbing fluid. Such transmission spectroscopy has a much higher detection sensitivity than the evanescent wave devices discussed earlier because the parameter f (which is a small number in the case of evanescent wave spectroscopy) does not appear in the absorbance value.

1.5 Fourier Transform Infrared (FTIR) Spectroscopy

1.5.1 FTIR Spectroscopy Theory

The key optical component of a Fourier Transform Infrared spectrometer is a Michelson interferometer consisting essentially of two mirrors and a beamsplitter as shown in Figure 1.8.

Figure 1.8 Michson interferometer

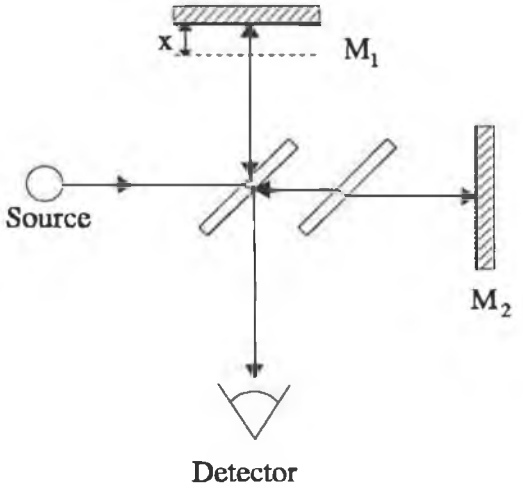

Both mirrors reflect the beams back to the beamsplitter where they are recombined. These two beams may add either constructively or destructively (if they are in phase or out of phase). A Michelson inteferometer varies the relative phase of one beam to the other by adjusting mirror $\mathbf{M_1}$. If the light source is monochromatic, scanning the movable mirror $\mathbf{M_1}$ causes the output beam intensity to rise and fall periodically, as the relative phase of the two recombining beams in the interferogram shifts. The frequency of the signal is proportional to the wavenumber of the monochromatic light source as discussed in Bomem (1989).

$$I(\delta) = \frac{I_0}{8} (1 + Cos(2\pi\delta\sigma)) \qquad \text{Eqn 1.10}$$

$I(\delta)$ = intensity measured for optical path difference δ in the interferometer.

σ = wavenumber of the light source = λ^{-1}.

I_0 = incident light intensity.

When the light source used contains many frequencies, the intensity measured

as a function of optical path difference is a summation (or in the limited case, an integral) over all frequencies ie.

$$I(\delta) = \int_0^\infty S(\sigma) \frac{I_0}{8} (1 + Cos(2\pi\delta\sigma)) \, d\sigma \qquad \text{Eqn 1.11}$$

The inteferogram measured by the spectrometer is

$$I(\delta) = \frac{I_0}{8} \int_0^\infty S(\sigma) \, Cos(2\pi\delta\sigma) \, d\sigma$$

Eqn 1.12

$$= \frac{I_0}{16} \int_{-\infty}^{\infty} S(\sigma) \, e^{i2\pi\delta\sigma} \, d\sigma$$

This is related to the frequency spectrum of the light by the fourier cosine transformation.

$$S(\sigma) = \int_{-\infty}^{\infty} I(\delta) \, e^{-i2\pi\delta\sigma} \, d\delta \qquad \text{Eqn 1.13}$$

For a more detailed discussion of Fourier Transforms see Brighan (1974).

Since "the spectrogram (irradiance versus wavenumber), of the light incident on a Michelson interferometer is the fourier transform of the inteferogram (irradiance versus path difference) as a function of mirror movement" it enables one by detecting the inteferogram $S(\sigma)$ to determine the spectral irradiance $I(\delta)$ as a function of wavenumber δ by fourier transform methods - see Pedrotti et al (1987).

The fourier transform methods mentioned refer in particular to the Fast Fourier Transform (FFT). The FFT is an algorithm that can compute the Discrete Fourier Transform (DFT) faster than other available algorithms as reported by Cochran et al (1967). Thus using the FFT, the DFT of the interferogram curve is calculated, giving the more familiar frequency spectrum.

The DFT takes the discretely sampled interferogram and performs a fourier transform on the data; this causes a problem if the sampling rate is not frequent enough. Wavelengths smaller than a λ_{min} show up as longer wavelengths in the spectrum. This phenomenon can be avoided by observing the Nyquist criterion ie. the spectrum must be sampled at a rate at least twice as high as its highest frequency component. The DFT also samples the data between two discrete points and not infinity, this causes sharp features such as absorption bands in spectra to be ringed by oscillations or "feet", this is referred to as aliasing due to data truncation. Aliasing can be reduced by using an apodization or "foot removal" function. Apodization consists of multiplying the inteferogram by a function that causes its intensity to fall to zero at its ends. The apodization function used with the "Bomem" MB-120 Michelson interferometer is a general-purpose cosine function.

$$F(\Delta) = \frac{1 + Cos(\pi\Delta)}{2} \qquad \text{Eqn 1.14}$$

Δ = optical path difference δ divided by maximum optical path difference
The use of different window or apodization functions eg. Bartlett (triangular) function have the same effect of reducing the side lobes in the frequency spectrum. See Rabiner et al (1975) for a detailed analysis of window functions.

As a result of all the manipulation detailed above, an extremely accurate means of collecting the frequency spectrum of the optical system of the Michelson interferometer exists. By placing a chemical species in the beam path of one of the arms of a Michelson interferometer, the frequency spectrum showing absorption lines or bands can be collected by referencing out the optical response of the system.

1.5.2 FTIR Spectroscopy Advantages

FTIR spectroscopy has two significant advantages over the transmission cell conventional spectrometer with grating or prism dispersion elements. The first is the so called *Jacquinot advantage* due to the large energy throughput (as distinct from the conventional spectrometer where entrance and exit slits of the monochromator restrict greatly the energy throughput). The second is the so called *Felgett advantage* due to

the simultaneous processing of the entire spectral range during a single scan of the instrument (ie. all wavelengths present reach the detector in the entire time required to observe a spectrum). This is in marked contrast to the ordinary dispersive spectrometer in which a particular wavelength is observed only during the brief interval in which it is incident on the exit slit of the monochromator and hence on the detector.

The total movement x of the moving mirror of the interferometer limits the resolution or bandpass σ (in cm^{-1}) that can be realised. The resolving power R defined by $\lambda/\Delta\lambda_{min}$ is thus δ/λ where $\delta = 2x$ since

$$\Delta\left(\frac{1}{\lambda}\right) = \frac{\Delta\lambda}{\lambda^2} = \frac{1}{\delta} \qquad \text{Eqn 1.15}$$

Giving

$$R \equiv \frac{\lambda}{\Delta\lambda} = \frac{\delta}{\lambda} \qquad \text{Eqn 1.16}$$

Thus a mirror movement of 5mm results in a resolving power of 20,000 at a wavelength of 500nm and a resolution of 0.025nm.

The simultaneous processing of all wavelengths of radiation make the FTIR less sensitive to source and detector fluctuations caused by mains power variations than its dispersion spectrometer relative.

1.6 Conclusions

The detection of chemicals using absorption spectroscopy with fibre optic sensors and fourier transform infrared spectroscopy was discussed; in particular the areas of mid infrared spectroscopy and the generation of absorption spectra by means of fourier transform methods. The transmission of mid infrared radiation to and from the sensing zone, along with various fibre probe designs for enhancing detection sensitivity were also presented.

CHAPTER 2

Chapter 2
Porous Clad Fibre Sensors

2.1 Introduction

When the cladding of an optical fibre is permeable to a chemical then its presence in the cladding may be detected via the attenuation of the evanescent waves of the guided modes. The reduction of the transmitted power of the guided modes in the presence of the chemical is a measure of the concentration of the species within the porous cladding. In this chapter the absorbance of a porous cladded multimode step index fibre is expressed in terms of the fibre core and cladding parameters and the properties of the chemical species, in particular teflon clad fibres. Also sol-gel overlayers and their sensitivity for gas detection are investigated. Measurements made with the teflon clad fibres and sol-gel overlayers used in conjunction with the FTIR spectrometer are discussed.

2.2 Porous Clad Fibre Theory

As discussed earlier the evanescent wave of a bound mode with propagation constant β and cladding parameter W $(= a\sqrt{\beta^2 - n_2^2 k^2})$ decays approximately exponentially in the cladding region as

$$\exp\left(-W\frac{r}{a}\right) \qquad \text{Eqn 2.1}$$

This gives rise to an optical power density $P(R)$ of approximately

$$P(R) = \frac{P}{\pi a^2 R} e^{-2V(R-1)} \qquad \text{Eqn 2.2}$$

where r = radial distance from core axis,

$R = r/a$ (a is the core radius).

The attenuation of a species of bulk absorption coefficient α in a cladding of

radius b and porosity[1] q as the chemical diffuses into the cladding has been treated by Ruddy (1993a). The fibre power loss (at an analytic wavelength) can be expressed as a time dependant attenuation coefficient $\gamma(t)$ given by

$$\frac{\gamma(t)}{\gamma_\infty} = 1 - \sum_n F_n \; e^{-\beta_n^2 T} \qquad \text{Eqn 2.3}$$

where $T = Dt/a^2$;t is time, D is diffusion coefficient of species in cladding material. The diffusion process is assumed to be Fickian.

$\beta_n = n\pi/(b/a-1)$ $\quad n = 1,2,3...$, provided $1 < b/a < 2$

F_n= a constant which involves the integral of the function $P(R)$ above and a Bessel function of the product $\beta_n R$.

- see Ruddy (1993a), Eqns 12, 13, 15. Represented graphically the time dependant attenuation coefficient is

Figure 2.1 Time dependant attenuation coefficient

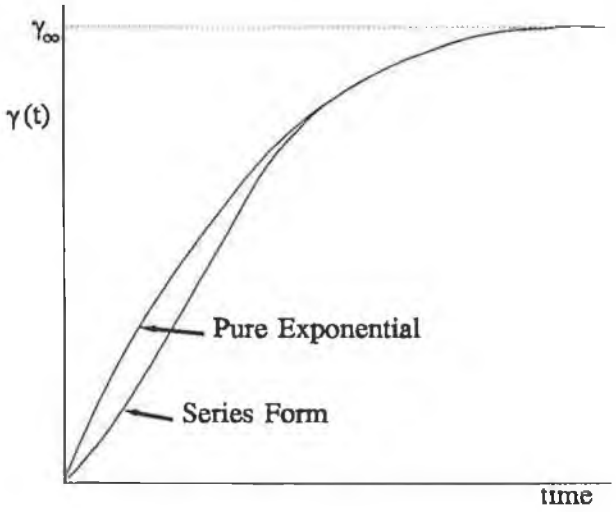

the function deviating from $1 - A\,e^{-ct}$ most pronounceably at small values of t. γ_∞ represents the steady state or saturation attenuation coefficient which is approximately

[1] The fractional volume of the cladding material that can be occupied (eventually) by the chemical.

$$\gamma_\infty = \frac{n_2 \alpha q}{n_1 V^2 \ln\left(\frac{b}{a}\right)} \qquad \text{Eqn 2.4}$$

For a weakly guiding fibre ($n_1 \simeq n_2$) with a thin cladding ($b \simeq a$) this reduces to

$$\gamma_\infty \sim \frac{\alpha q}{V^2 (b/a-1)} = \frac{\alpha a q}{V^2 d} \qquad \text{Eqn 2.5}$$

where $d = b-a$ is the cladding thickness. Thus the theory predicts that the equivalent length of the fibre probe of length L is

$$L_{eqv} = \frac{Laq}{V^2 d} \qquad \text{Eqn 2.6}$$

where L_{eqv} is the equivalent length.

This means that a porous fibre probe of length L will attenuate the transmitted power (as $t \rightarrow \infty$) by an amount equal to that of a transmission cell of length Laq/V^2d. As V is typically a large number (100 or greater) the transmission cell equivalent length is much smaller than that of the fibre probe which gives rise to the same absorption. The expression quoted above assumes that

i) the chemical diffuses into the cladding pores obeying Ficks law

ii) the chemical does not modify the refractive index n_2 of the cladding; this can however be allowed for fairly easily.

For the case of gases ($n \simeq 1.0$) diffusing into the cladding the local numerical aperture of the fibre $(n_1^2-n_2^2)^{1/2}$ will not change and as a result the V number will be a constant. For the case of liquids the local numerical aperture will decrease leading to a reduction in the V number. This will result in an attenuation coefficient which is no longer linearly dependant on the value of α ie. no longer linearly dependant on the concentration of the species. This effect has been reported by De Grandpre and Burgess (1990) for the case of the diffusion of toluene into a siloxane clad silica fibre.

2.3 Experimental Setup

2.3.1 Fourier Transform Infrared (FTIR) Spectrometer System

The FTIR spectrometer used in the system was a Bomem "Michelson series" MB-120, which is a continuous scan Michelson interferometer. The instrument has a wavenumber spectral range of 5,000cm^{-1} to 400cm^{-1} (2μm to 25μm), which is limited on the lower wavenumber range by the transmission properties of the Potassium Bromide (KBr) windows and beamsplitter. The spectral range is further limited by the choice of detectors. Initially a Deuterated Triglycine Sulfate (DTGS) detector with a range of 5,000cm^{-1} to 400cm^{-1} or 2μm to 25μm was used. This made effective use of the full spectral range of the system, but was not sensitive enough to detect the low light levels launched into single and few mode optical fibres. The present system incorporates a high sensitivity liquid nitrogen cooled Indium Antimonide (InSb) detector (see Figure 2.2) with a reduced spectral range of 5,000cm^{-1} to 800cm^{-1} which is further reduced by a noice reduction filter to a range of 5,000cm^{-1} to 2,200cm^{-1}; as we are interested in the region of 3,000cm^{-1} to 4,000cm^{-1} (absorption region of CH and OH bonds) this is still satisfactory.

The FTIR used has a variable spectral resolution from 1cm^{-1} to 128cm^{-1} in steps of powers of 2 and an open beam (no attenuator present) signal to noise ratio of 500:1, obtained from a transmittance spectrum at a resolution of 4cm^{-1} and a wavenumber of 2,000cm^{-1} for a 20 second observation time using a DTGS detector. It also has a stability of 0.1% standard deviation at 2,000cm^{-1} for ratioed consecutive open beam spectra - see Bomem (1989). One essential function of spectrometers in that they increase the signal to noise ratio by integrating spectra. The amount of noise present in a spectrum is inversely proportional to the square root of the signal averaging time. For example, a spectrum produced by acquiring 50 sample and reference interferograms will have approximately one fifth the noise level of a spectrum produced from two sample and reference interferograms, because 50/2 = 25 times as much time was spent in measurement.

There is a pre-amplifier associated with each detector used with the system.

Figure 2.2 Specific responsivity D* as a function of wavelength for a number of representative photodetectors (Wilson 1983).

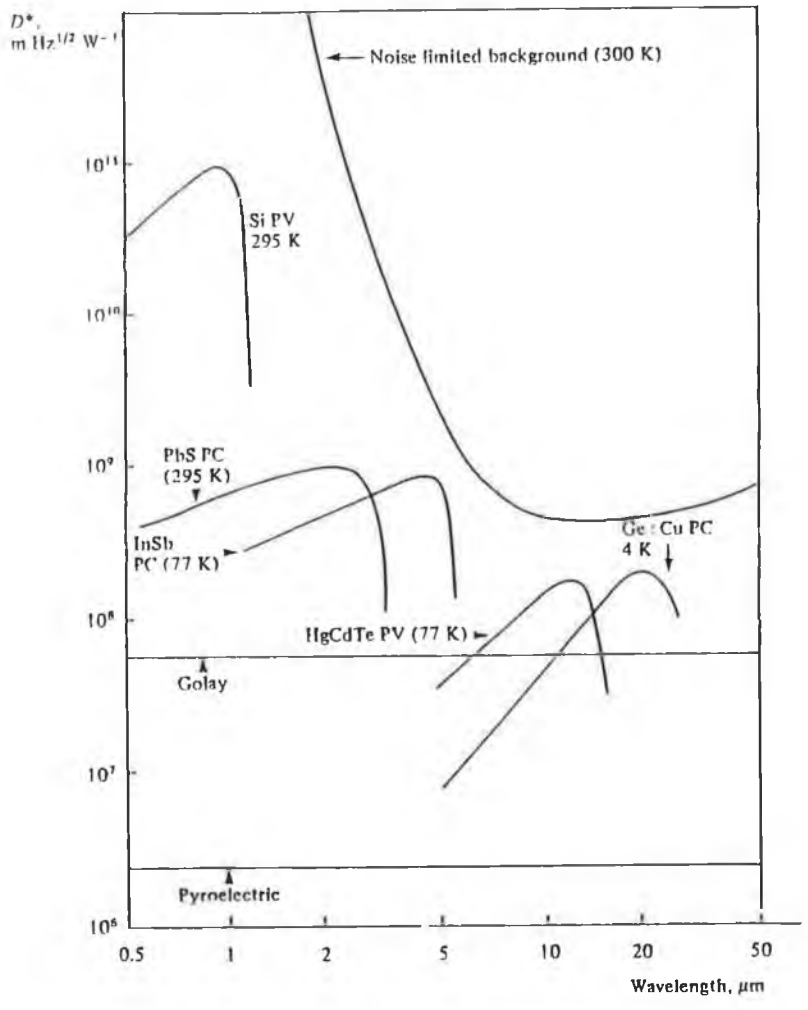

DGTS is a Pyroelectric detector (PC = photoconductive, PV = photovoltaic).

Thus a gain of 1x, 2x, 4x, 8x and 16x can be selected by means of a rotary switch. The 1x gain position is factory calibrated so as to feed 4.5 volts to the Analog to Digital Converter (ADC) under maximum possible signal conditions (open beam). All the other gain positions are uncalibrated and as such the intensity units of the spectrum are arbitrary. This in no way affects the Transmittance or Absorbance spectra as they are ratioed against the Reference spectra.

The instrument uses a ceramic broad-band high intensity source which is temperature stabilized. The Michelson interferometer consists of a KBr beamsplitter

as mentioned above and surface coated cube mirrors - see Figure 1.8. A Helium-Neon laser is used to measure mirror scan position and a wavenumber precision of $0.01cm^{-1}$ is achieved. The Michelson interferometer uses a low noise 16 bit analog to digital converter (ADC) in conjunction with a Digital Signal Processing (DSP) card to transform the inteferogram (irradiance versus path difference) to its spectrogram (irradiance versus wavenumber) which is then recorded by a NEC "Power-Mate 286 Plus" personal computer with maths coprocessor.

Figure 2.3 FTIR system diagram

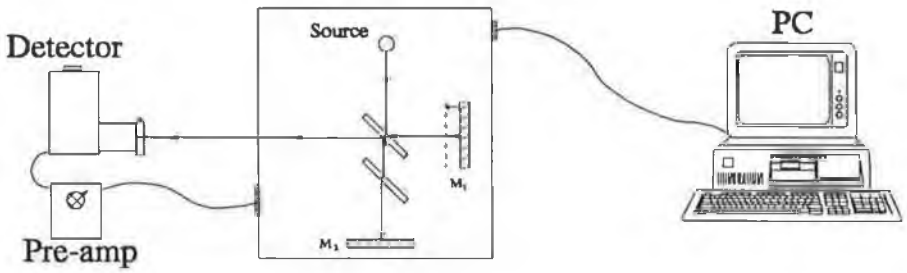

2.3.2 Optical Fibre Launch/Collection System

The optical side port of the FTIR spectrometer was used in conjunction with suitable lensing to launch into the optical fibres. Lensing was used despite the chromatic dispersion associated with lenses when used with broad band sources, due to the variation of the refractive index of the lens with wavelength. Lenses were preferred over parabolic mirrors as they were far more efficient in terms of power launched, even though parabolic mirrors have no chromatic dispersion.

Figure 2.4 Optical fibre launch/collection schematic

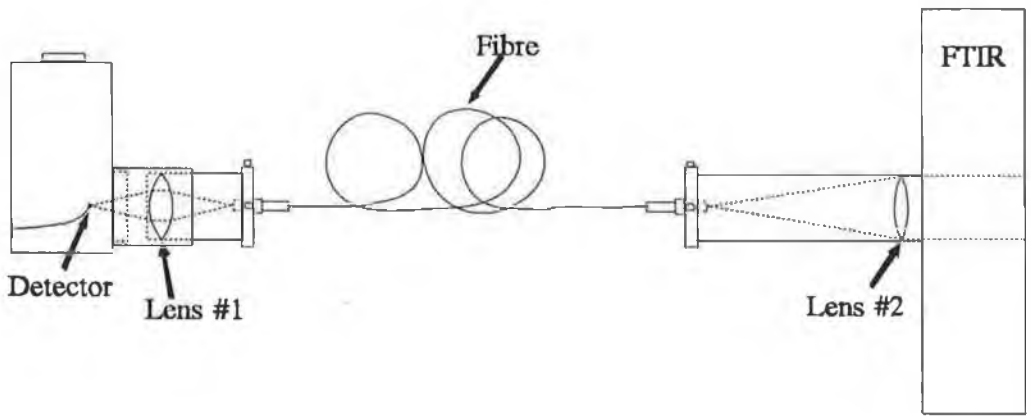

The FTIR spectrometer delivers an approximately parallel beam of IR radiation from its optical side port. The Bomem specifications state a divergence of 40 mrads. The divergence was measured at 33.4 mrads and the total output power was measured at approximately 0.02 Watts; this includes power from all wavelengths as a broad band pyroelectric detector was used in the measurement. The FTIR spectrometer output beam is captured and focused by Lens#2 (see Figure 2.4), which is a 25mm diameter ***d*** Calcium Fluoride (CaF_2) IR transmitting lens with a focal length f of 100mm, giving an f-number of 4. Using

$$f\# = \frac{f}{d} = \frac{1}{2NA} \qquad \text{Eqn 2.7}$$

This gives an effective[2] launch NA of 0.125, which is ideally suited as the fibres used have a similar NA. Thus the optical power launched is maximised by matching the NA of the fibre and the launching optics. It was noted that the spot size generated by this setup was of the order of a two centimeters instead of 60μm as predicted by the diffraction limited case. This agrees with the two centimeter spot size predicted by a ray tracing package when chromatic dispersion and the slight divergence of the input beam are taken into account.

The launched light is transmitted to the detector by means of an IR fibre and collected by Lens#1 a 25mm diameter Calcium Fluoride (CaF_2) IR transmitting lens with a focal length of 20mm. Thus by placing the fibre and the detector both at twice the focal length ($2f$) from the lens, all the emitting light from the fibre should be focused on the detector with a magnification of one. Given that the largest fibre core diameter used is less than 300μm and the detector area is given as $1mm^2$ all emitted light should be collected. With the fibre placed at 40mm ($2f$) this gives an effective collection NA of 0.3, which is more than sufficient for any of the fibres used. Newport fibre chuck positioners are used to align both fibre ends so as to maximise the power throughput for a given wavenumber region. The chromatic dispersion causes different wavelengths to be focused in different areas, thus by moving the fibre the wavenumber region of interest can be selected preferentially.

---

[2]Effective launch NA is 0.125 when the fibre is placed at the focus of the lens

2.4 Polymer Clad Fibres

2.4.1 Polymer Clad Experimental Setup

The experimental arrangement shown in Figure 2.5 consisted of the launch and collection optics as detailed in section 2.3.2 as well as the FTIR spectrometer and personal computer discussed in section 2.3.1.

Figure 2.5 Porous clad fibre experimental setup

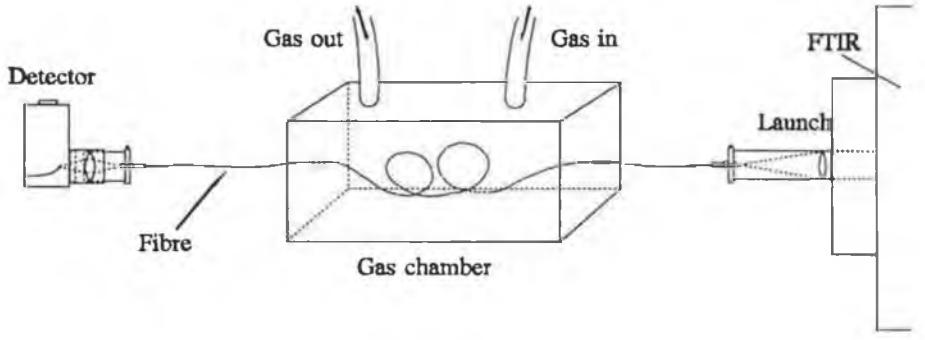

The optical fibre used was a zirconium fluoride IR transmitting fibre with a teflon cladding. The core/cladding ratio was 280/300μm which gave a 10μm cladding thickness. The Teflon clad fibre was passed through a gas chamber and then the cleaved fibre ends were placed in fibre chucks which were then aligned using the three dimension (x, y, and z) positioners. A reference spectrum was done with the gas chamber filled with Nitrogen (N_2). A transmission scan was done later with the gas chamber filled with 100% propane (C_3H_8). The final transmission spectrum is achieved by taking the reference spectrum and dividing each point by the equivalent point in the spectrum achieved with the propane in situ. Thus by ratioing the two spectra as mentioned means zero absorption is represented by 100% transmission and vice versa. By this means the characteristic spectrum of propane and the percentage absorption achieved with polymer clad fibres can be recorded. This data is then stored automatically on the personal computer for future analysis.

It should be noted that any memory effects associated with gas adsorption to the sensor probe glass surfaces is compensated for as each gas spectrum is compared to a "no gas" spectrum. Should the latter have any structure due to gas retention in the sensor the referencing procedure would remove the effect.

2.4.2 Experimental Results and Analysis

Porous clad fibre probes were used together with the FTIR spectrometer in the detection of propane gas. The probes consisted of Teflon clad fluoride fibres of the following dimension:

Core radius a = 140μm

Cladding radius b = 150μm

Numerical aperture NA = 0.6

Fibre V number = 160 (at λ=3.3μm)

Active zone length L = 0.33m

and the following transmittance spectrum was obtained for 100% propane[3]

Figure 2.6 Propane spectrum using porous clad fibre

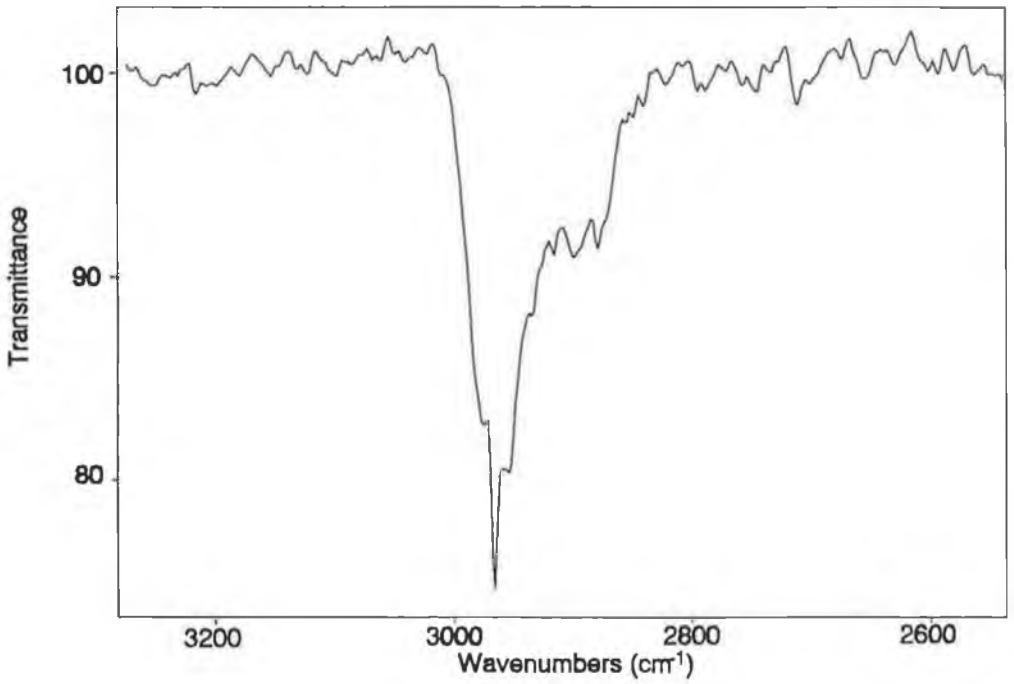

The 75% transmittance observed predicts a fraction f of the optical power in the cladding region given by

$$e^{-f\alpha z} = 0.75 \qquad \text{Eqn 2.8}$$

where α is the bulk absorption coefficient of propane at 3.3μm and z is the active

[3]Small amounts of Isobutane, N-butane and Pentane were also present in the gas.

length of the sensor probe. The value of α for propane at a $1cm^{-1}$ resolution can be deduced from data published by Erley and Blake (1965) to be $1150m^{-1}$. Using this and $z = 0.33m$ the value of f predicted is then $7.58x10^{-4}$.

Taking the fibre V number as 160, the launch NA_L as 0.125, and the fibre NA_F as 0.6 the theoretical model of Ruddy (1990b) predicts a fractional power value f of

$$f = \frac{1}{V}\frac{NA_L}{NA_F} = 13.02 \; x \; 10^{-4} \qquad \text{Eqn 2.9}$$

The discrepancy of a factor of approximately 2 between the measured and theoretical values may be due to the fact that the value for α used was derived from measurements at a spectrometer resolution of $1cm^{-1}$ while our experimental data was based on an FTIR resolution of $4cm^{-1}$.

The linewidth of a single rotational-vibrational transition for a gas (at 300K) is a narrow gaussian of typically $0.01cm^{-1}$ full width at half maximum. At STP intermolecular collisions give rise to a doppler broadening with a resultant Lorenzian lineshape of full width at half maximum of typically $0.1cm^{-1}$.

If the resolution of the spectrometer is narrower than the linewidth of the material being detected then obviously the true linewidth of the transition is observed. However if the resolution of the spectrometer is wider than that of the material being detected the observed spectrum will appear broader and less intense. In the context then of propane absorption at 3.3μm the Erley and Blake value of $1150m^{-1}$ for the attenuation coefficient measured at $1cm^{-1}$ resolution is smaller than the figure which pertains to the intrinsic linewidth of the transition. The value relevant to our measurements with a $4cm^{-1}$ resolution should be smaller still. In Eqn 2.8 then α is smaller than $1150m^{-1}$ to achieve 75% transmittance and so f must be larger. This is in keeping with the results discussed earlier.

2.5 Sol-gel Overlayers

2.5.1 Experimental setup

One of the standard methods of evanescent wave liquid sensing involves polishing down of the fibre cladding as reported by Mazé (1989). This enhances the evanescent power that can interact with the liquid to be sensed. The fibre is placed on a curved block and a hardening solution is poured over the fibre to give structural support while polishing. The surface is then polished down until only a very thin cladding layer is left at the highest point of the arc as shown in Figure 2.7.

The polished fibre block used was a single mode 11/125μm fibre system supplied by "Le Verre Fluore (France)" . The fibre came prepolished and connectorised, but to enhance sensitivity the fibre was further polished as part of another research project. This allowed us to deposite a sol-gel overlayer on a specially prepared polished fibre block with increased sensitivity.

Figure 2.7 Polished fibre with Sol-gel overlayer

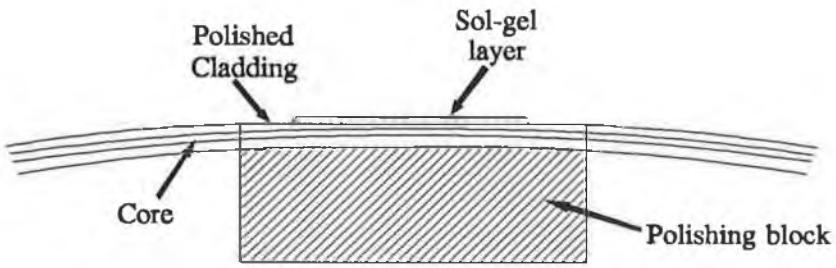

The sol-gel overlayer was deposited at Trinity College Dublin by the M°Gilp group. The sol-gel deposited is a silica based sol-gel and as such is not ideally suited for use with zirconium fluoride fibres, due to the refractive index of silica being 1.46 and zirconium fluoride being 1.5 approximately.

The experimental setup used for the sol-gel overlayers is the same as that used for porous clad fibres in section 2.3.3 except for the active sensing region. In the sol-gel overlayer case the sensing region consists of the previously mentioned fibre polished block with sol-gel overlayer to further enhance sensitivity.

Figure 2.8 Sol-gel overlayer experimental setup

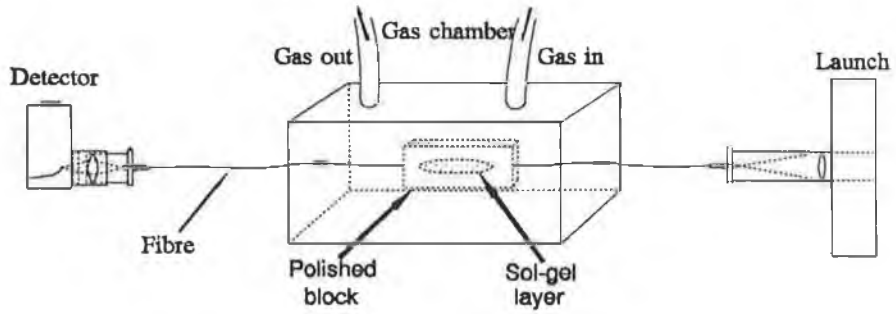

100% propane (C_3H_8) as used in the polymer clad fibre experiments was then pumped in to the gas chamber and left to diffuse into the solgel overlayer. The propane was pumped in at pressure to ensure that the gas had diffused into the sol-gel totally. This was done as the sol-gel overlayer was approximately 0.5mm thick, which gives a total cladding of over 500μm making it essential that the gas travel through most of the sol-gel overlayer before encountering the evanescent field associated with the propagating mode of the single mode fibre. The propane was then reduced to one atmosphere pressure and a transmission spectrum was recorded (Figure 2.9) using a previously recorded spectrum of 100% Nitrogen (N_2) as the reference.

A feature of the FTIR spectrometer controlling software is the ability to do timed multiple scans. This allowed us to take transmission spectra with a controlled time interval, showing the diffusion of the gas (reduced transmission) into the sol-gel overlayer with respect to time - see Figure 2.10.

2.5.2 Experimental Results and Analysis

The sol-gel overlayer deposited on the polished fibre block was used in conjunction with the FTIR in the sensing of propane gas. The Sol-gel being silica based with a refractive index of 1.46 causes the refractive index of the sol-gel when in contact with a gas to be approximately 1.23 assuming 50% porosity ie. (1.46+1.0)/2. The 50% porosity in return reduces the concentration of the gas from 1.0 to 0.5. The refractive index gain and the reduction in concentration counter balance each other, but when theoretically analysed by M^{c}Cabe (1993), it was shown that a gain of 2 could be expected. If the sol-gel is in the presence of a liquid the

refractive index change is from 1.33 to 1.395 (0.065 change) and the concentration is still reduced to 0.5. The same theoretical analysis gives no expected gain when a sol-gel overlayer is used, as opposed to a polished block with no overlayer present.

The polished block without an overlayer was found to be sensitive to liquids giving approximately 100% absorption for propanol, but no sensitivity to gases was found. This was as expected as the large refractive index difference between the polished block and the gas as well as the lower attenuation coefficient of gases than liquids gives a sensitivity ratio of 100:1, ie. it is 100 times easier to sense liquids using evanescent field methods, as shown in Figure 5 of Mac Craith et al (1991).

Using the sol-gel overlayer no gain was achieved for liquids as predicted, but 9% absorption was achieved for 100% propane - see Figure 2.9 - which represents a gain of greater than 2 ie. absorption went from <2% to 9%.

Figure 2.9 100% Propane spectrum using the sol-gel overlayer

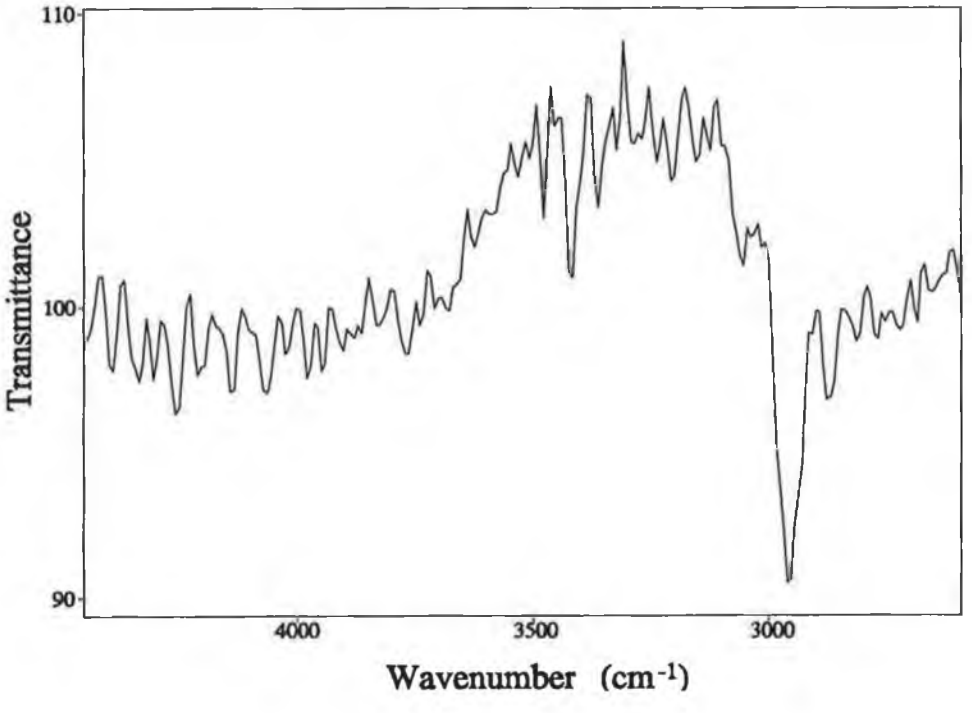

This result gives an ideal starting point for future work with sol-gel overlayers. The purpose of our experiment was to establish the feasability of sol-gel overlayers in relation to gas sensing via evanescent field enhancement and to prove that the

theoretical gain could be achieved. Due to the fact that many of the sol-gel layer and polished block parameters were unknown the experimental absorption can not be compared to a theoretical predicted absorption.

A negative feature of sol-gel overlayers, as with all porous claddings, is the delay due to diffusion of the gas or liquid reaching the sensing zone (the core/cladding interface). It can be seen from Figure 2.10 for propane diffusion into a sol-gel cladded fluoride fibre that the absorption continues to increase with time. This implies that the rate of diffusion into the sol-gel overlayer is slow, possibly due to small pore diameter in relation to the size of the propane molecule (C_3H_8).

Figure 2.10 Propane diffusion into sol-gel overlayer

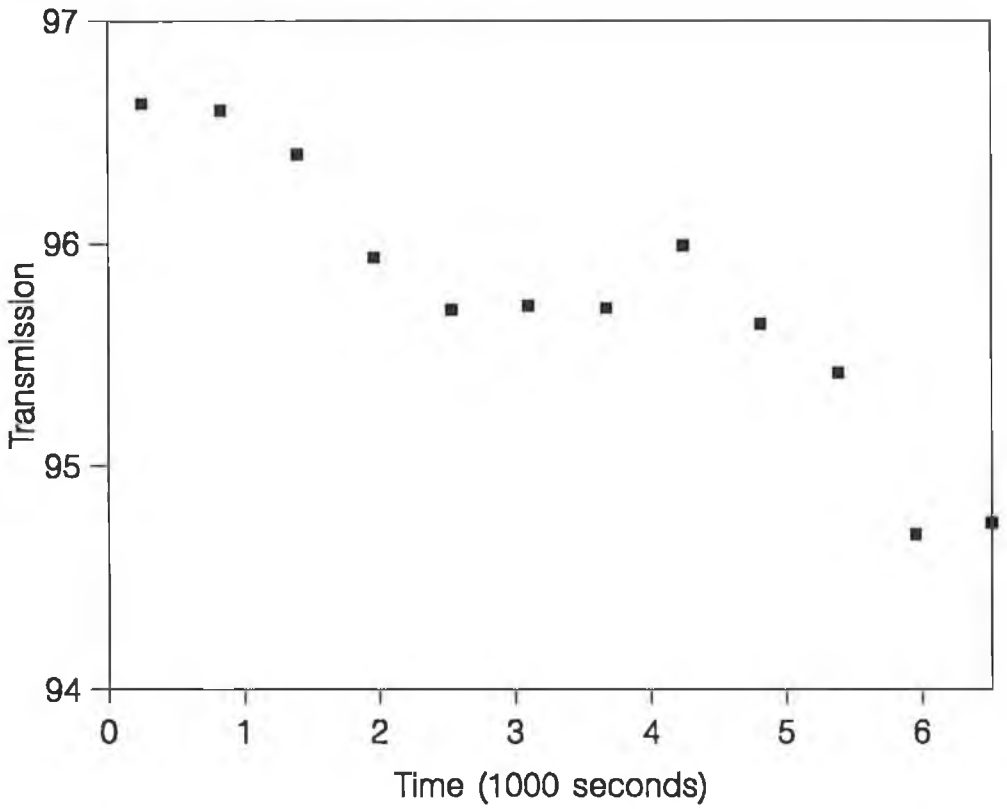

In the diffusion process saturation occurs when

$$\frac{D\,t}{(b-a)^2} >> 1 \qquad \text{Eqn 2.10}$$

thus for non-saturation

$$\frac{D\,t}{(b-a)^2} << 1 \qquad \text{Eqn 2.11}$$

$$\Rightarrow D << \frac{(b-a)^2}{t} \qquad \text{Eqn 2.12}$$

Taking the cladding thickness b - a in the sensing region to be 0.5mm and a saturation time of more than 6500 seconds - Figure 2.10 - an estimate of the upper limit of the diffusion coefficient D of propane in the sol-gel used may be made. A value of $D < 5\text{x}10^{-11}\text{m}^2/\text{s}$ is obtained. Typical diffusion coefficient D values according to Brandrup (1979) for propane diffusion into polymers are

Table 2.1 Polymer Diffusion coefficients for propane (C_3H_8)

Polymer	D m^2/s
Polyisoprene (natural rubber)	2.1×10^{-11}
Perbunan (73/27)	1.4×10^{-11}
Polyisobutene-co-isoprene	2.2×10^{-12}
Polytetrafluoroethylene (Teflon)	7.7×10^{-14}

The Diffusion coefficient D value of less than $5\text{x}10^{-11}\text{m}^2/\text{s}$ (large D means short diffusion time) for propane diffusion into the sol-gel overlayer implies that the diffusion rate is of the same order of magnitude as that for polymers in general. The advantage of sol-gels is that the pore size can be varied, so as to increase the diffusion rate. This would enable more rapid and more realistic gas sensing time scales.

2.6 Conclusions

Two fibre sensing systems were discussed. In one the porous cladding of a polymer clad fluoride fibre is used as the sample cell for evanescent wave spectroscopy, in the other a sol-gel layer located locally on an exposed section of fibre core acts as the matrix for gas detection also by evanescent wave absorption spectroscopy. The theoretical and experimental results for both sensing systems were

in rough agreement, with absorptions of 25% and 9% respectively for 100% propane. The only disadvantages of these methods of gas detection are the need for the gas to diffuse to the sensing zone and possible residual effects due to the pressence of some of the sensed gas remaining in the porous cladding.

CHAPTER 3

Chapter 3
Fibre Tapers

3.1 Introduction

The tapering of a section of optical fibre in order to enhance optical power in the evanescent wave is a technique used in the manufacture of fibre optic couplers. For identical reasons multimode and singlemode step index fibre may be tapered to fabricate evanescent wave sensing probes. In this chapter work carried out on multimode and single-mode fibre tapers for a chemical probe suitable for use with an FTIR spectrometer will be discussed.

3.2 Taper Fabrication

The basic principle of fibre taper manufacture is the heating of the fibre followed by stretching in both directions to form a narrow taper waist which is linked to unstretched fibre by a conical section at each end.

Figure 3.1 Taper drawing method

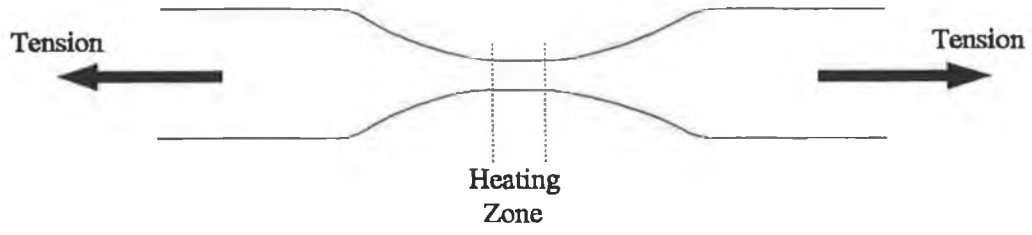

Such tapers are called biconical and give a symmetrical taper diameter versus position profile about the centre of the taper. Asymmetry arises if one end of the fibre is held fixed while applying tension to the other as shown by Bobb et al (1990). The optical properties of the waveguide change from an effective infinite cladding of glass to the centre of the taper where the surrounding medium, normally air, acts as the cladding and the remaining glass forms the new fibre core. In the case of fibre taper probes the cladding in the taper waist is the chemical being sensed. If such a taper is made slowly enough then little or no optical power is lost, resulting in an adiabatic

taper. Criteria for such adiabatic tapers have been developed by Love et al (1991).

The taper shape is determined by the heating zone and it has been shown by Birks and Li (1992) and Kenny et al (1991) that a travelling burner may be used to produce a hot zone and to fabricate any "reasonable taper shape" for silica fibre.

The manufacture of fibre tapers from step index 60/90μm multimode fluoride glass fibre was tried using a tapering rig constructed by Curran (1992) which consists of a silica glass flow cell through which the fibre is threaded and anchored to the two translation stages driven by a stepping motor. The flow cell is surrounded by a resistive heater which is temperature controlled using a thermocouple located within the cell in the proximity of the fibre which is kept in a nitrogen atmosphere during the drawing process. A drawing temperature of 285°C approximately was found suitable for the fluoride fibre.

Figure 3.2 Tapering rig

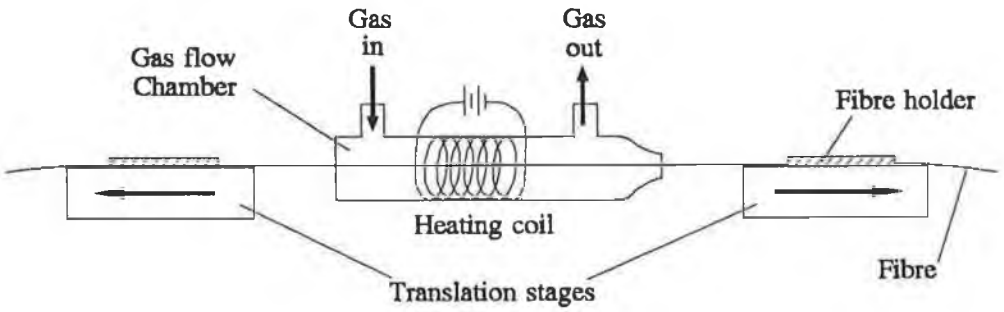

3.3 Theory

The simplest model of a tapered fibre evokes conservation of mass (or volume) in a length *W* of fibre which is heated to show that diameter reduces exponentially with position as discussed by Tekippe (1990). His diagram and equations are reproduced in Figure 3.3 and Eqn 3.1; these agree with Dewynne et al (1989) and Eisenmann et al (1988) among others. This is sometimes referred to as the constant hot zone method of tapering.

Figure 3.3 Taper Geometry - Tekippe (1990) -

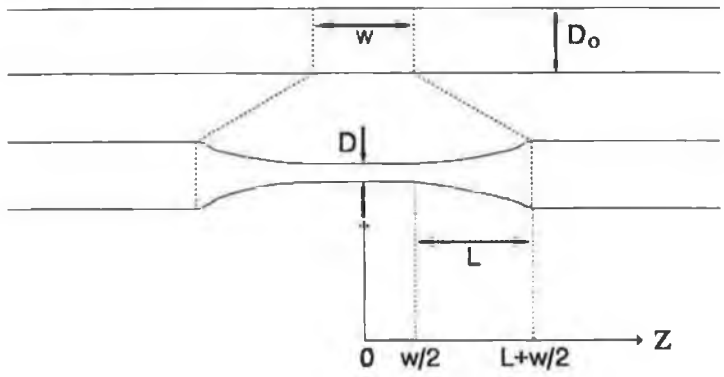

$$D = D_O \exp\left(\frac{-L}{w}\right)|Z| \qquad z \le \frac{w}{2}$$

$$D = D_o \exp\left(\frac{|Z| - L - \frac{w}{2}}{w}\right) \qquad \frac{w}{2} \le |Z| \le L + \frac{w}{2} \qquad \text{Eqn 3.1}$$

$$D = D_o |Z| \qquad z \ge L + \frac{w}{2}$$

Birks and Li (1992) show that where the hot zone length changes linearly with the taper extension.

$$L(x) = L_o + \alpha x \qquad \text{Eqn 3.2}$$

the resulting taper profile is

$$r(z) = r_o\left[1 + \frac{2\alpha z}{(1-\alpha)L_o}\right]^{\frac{-1}{2\alpha}} \qquad \text{Eqn 3.3}$$

In the case of α = -0.5 ie. the hot zone shrinking at half the rate of taper extension or elongation the resulting profile is linear

$$r(z) = r_o\left[1 - \frac{2z}{3L_o}\right] \qquad \text{Eqn 3.4}$$

Varying the value of α creates a whole family of taper types as shown in Figure 4 of Birks and Li (1992) paper reproduced below in Figure 3.4.

Figure 3.4 Taper profiles with varying α - Birks and Li(1992) -

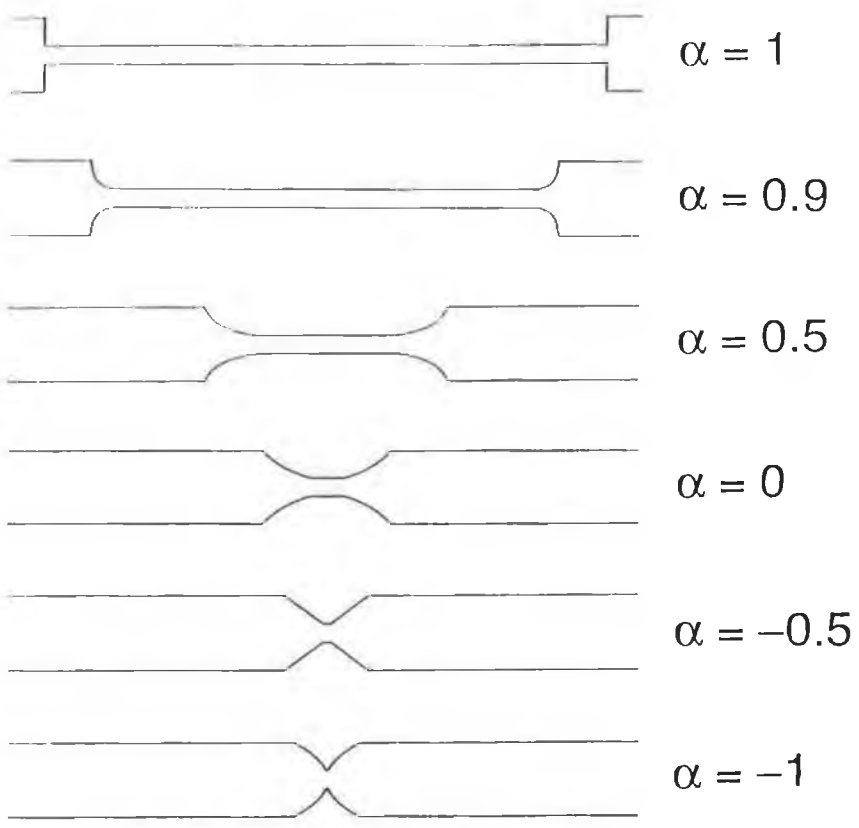

For sensor applications abrupt changes in taper diameter cause an appreciable loss of optical power from the fibre leading to low detection sensitivity. The negative alpha values shown in Birks and Li (1992) paper exhibit such sharp transitions.

Using a travelling gas burner which produces a narrow (~2mm wide) flame which is moved up and down the fibre "in the manner of a flame brush" Birks and Li manufactured tapers that matched the predictions of their model. This they attribute to the burner simulating "the ideal uniform temperature profile of the model, with each fibre element within the transversed length being heated and stretched equally".

3.4 Taper characterisation

The tapers pulled using the experimental setup mentioned above were found to be unable to sense chemicals. The taper shape when viewed under a microscope was not smooth, this led to non-adiabatic tapers which lost optical power as one

tapered. Thus as the sensitivity increased, the noise in the spectrum increased making any spectral detail impossible to view. The uneven tapering also made it impossible to pull narrow sensitive tapers. The possible cause of this uneven tapering was thought to be non uniform tension applied during tapering, as our method involved a constant pull rate rather than constant tension during tapering. It was theorised that the uneven profile was due to a build up of tension with constant pull rate to a point where the force is enough to cause tapering. This releases the tension on the fibre and tapering stops until another build up of tension causes the fibre to taper again and so on. This conclusion was based on the fact that all other parameters were varied in our tapering process and the basic problem remained. Thus to get effective zirconium fluoride tapers a PID (Proportional Integration Differentiation) control system should be used to control fibre tension during tapering as used in industrial manufactured tapers.

An industrial manufactured taper probe was supplied by "Le Verre Fluore" France from 11/125μm fibre. The diameter versus position profile of the zirconium fluoride single-mode taper was examined under a microscope and found to be approximately linear. The taper waist was 28mm length and 15μm diameter with a gradient ϕ of 0.053° over a length of approximately 12mm, see Figure 3.5. An overall fibre diameter reduction of 88% was achieved.

Figure 3.5 Single-mode taper profile

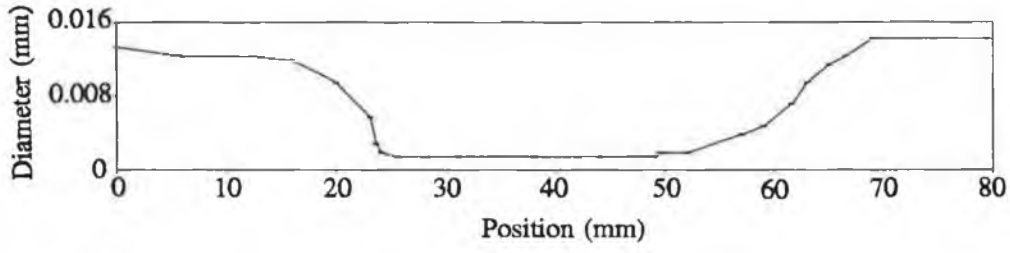

The assumption of a linear taper (ϕ being constant) may be used to predict the variation of the axis crossing angle θ_z of a ray (or mode) in the fibre taper region with location as

$$\theta_z = \theta_o + 2n\phi \qquad \text{Eqn 3.5}$$

where θ_o is the initial axis crossing angle of the ray and θ_z the value after n reflections on the surface of the taper according to Ruddy (1993b). Eqn 3.5 indicates that as a mode propagates in a taper θ_z increases indicating an increase in the order of the mode, or in other words its approach to cut off.

For the 11/125μm fibre used the V number at the wavelength of interest (3.3μm) for an NA of 0.125 is 1.309; this being less than 2.405 indicates that there is only one mode present. Using Table 14.4, pp 315 of Snyder and Love (1983) the core mode parameter U is approximately 1.20 ie.

$$U = a\sqrt{n_1^2 k^2 - \beta^2} = 1.20 \qquad \text{Eqn 3.6}$$

Using $a = 5.5\mu m$

$k = 1.904\mu m^{-1}$

$n_1 = 1.50$

we get $\beta = n_1 k \cos\theta_z = 2.848$

or $\theta = 4.38°$

ie. the fundamental mode crosses the untapered lead-in fibre axis at an angle of 4.38°. This corresponds to θ_o in Eqn 3.5. Each time the ray crosses the tapered section θ is incremented upwards by 2ϕ or about 0.106° in this case. A knowledge of n, the total number of reflections in the tapered section can then be used to determine θ_z of the ray in the waist region of the taper. This value of θ_z will be used later to theoretically model the taper sensitivity to propane.

3.5 Experimental Results and Analysis

The fibre taper probe was coupled to the side port of the Bomem FTIR spectrometer using CaF_2 lens optics detailed in section 2.3.2. The experimental system involved the use of a specially designed glass gas cell which provided support for the delicate taper as well as providing a means of filling and extracting gases from

the taper environment as shown in Figure 3.5. This structure also comprised of reinforced lead-in connectorised fibres.

Figure 3.6 Fibre taper probe

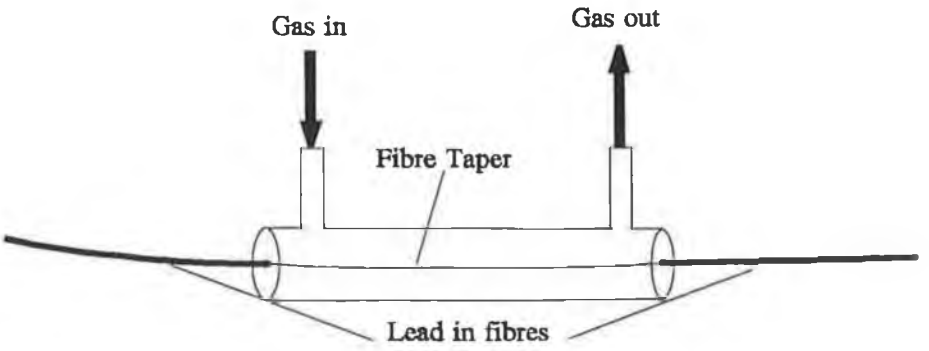

With the instrument resolution set at 16cm^{-1} a reference spectrum of the fibre taper probe was recorded. To increase the signal to noise ratio the reference spectrum was integrated for 500 scans. Then a transmission spectra of 500 scans with 100% propane present in the gas chamber was done. Using the Bomem software the spectra were ratioed to give the transmission spectrum of propane as shown in Figure 3.7

Figure 3.7 100% Propane spectrum using the single-mode taper probe

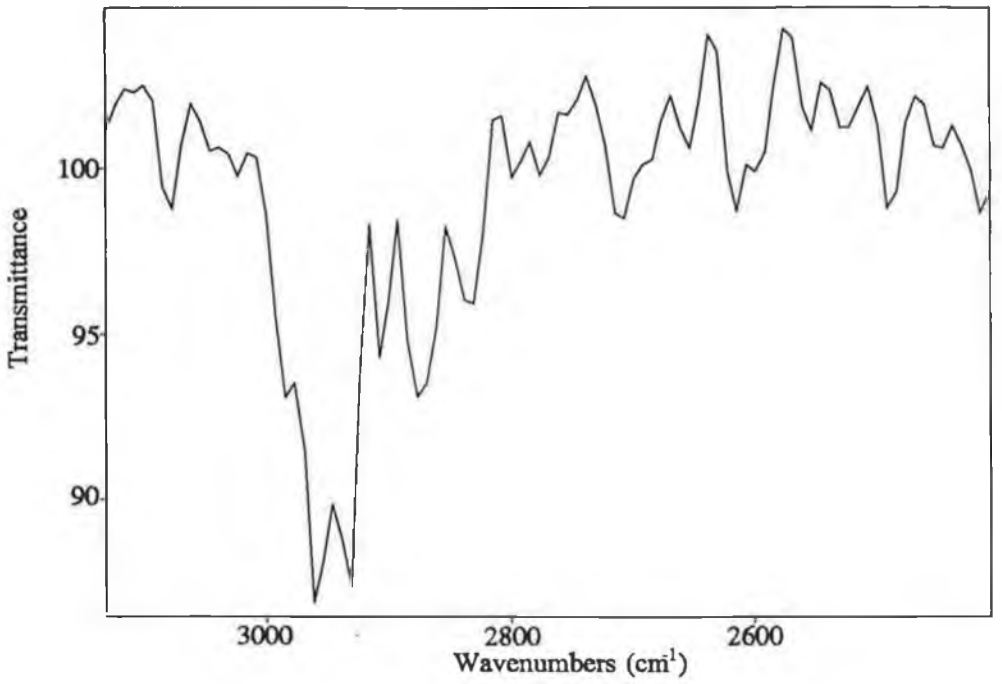

As can be seen a strong absorption of 13% or a transmittance of 87% can be seen at 3.36μm or 2975cm^{-1} corresponding to C-H vibrational frequency characteristic

of hydrocarbons.

As stated earlier a knowledge of n, the total number of reflections in the tapered section may be used to determine θ_z of the ray in the waist region of the taper. An estimate of the value n may be obtained using the number of reflections per unit length N expression for a fibre as stated in Snyder and Love (1983), Eqn 1-11 pp 11.

$$N = \frac{Tan\theta_z}{2a} \qquad \text{Eqn 3.7}$$

In the case of the taper used the core diameter is originally 11μm with a cladding of 125μm diameter. The cladding becomes in the taper waist a 15μm diameter glass core clad with air. As both θ_z and the core radius a vary along the taper we can get a lower estimate of N by taking a = 5.5μm and θ_z = 4.38° in Eqn 3.7. This gives N_{min} = 6,963 reflections per metre or approximately 84 in the 12mm length of tapered section, Figure 3.8. Using Eqn 3.6 then the ray crossing angle on reaching the waist region is

$$\theta_z = 4.38 + 84(0.106) = 13.28^o$$

Figure 3.8 Taper schematic

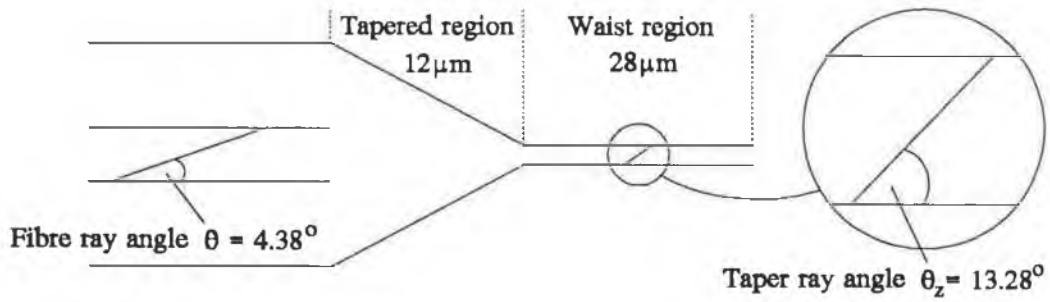

If the fractional power loss at each reflection in the waist region is given by T^* then the transmittance of the waist region, when surrounded by an absorber of bulk absorption coefficient α is

$$T = e^{-NT^*L} \qquad \text{Eqn 3.8}$$

according to Eqn 6-17, pp 126 of Snyder and Love (1983) with

$$T^* = \frac{\alpha \lambda n_2 \, Sin\theta_z}{\pi\left(n_1^2 - n_2^2\right)\sqrt{Cos^2\theta_z - (n_2/n_1)^2}} \qquad \text{Eqn 3.9}$$

For the taper used surrounded by 100% propane gas the following values are used

$\alpha = 900m^{-1}$

$n_1 = 1.50$

$n_2 = 1.0$

$\lambda = 3.3\mu m$

$\theta_z = 13.28^o$

and yields a value of T^* of $2.45x10^{-4}$. Using Eqn 3.8 then the transmittance of the fibre taper waist surrounded by undiluted propane is predicted to be

$$T = \exp\left[-(15734)(2.45x10^{-4})(28x10^{-3})\right] = 0.897$$

where 15,734 is the number of reflections per metre in the waist region, derived from Eqn 3.7. The experimental transmittance of the taper at $2975cm^{-1}$ or $3.36\mu m$ in the presence of propane gas is shown in Figure 3.7. It can be seen that the experimentally determined transmittance of ~87% is not substantially different from the theoretical value of 89%. In view of the many assumptions used in the derivation of the theoretical model the correlation between theory and practise is remarkably good.

Taking a minimum detectable transmittance of 95%, assuming a 5% absorption is the minimum detectable, the taper used (28mm of 11/125μm fibre drawn to a 15μm waist) the minimum detectable concentration can be calculated to be about 47% propane by volume. To reach a lower explosion limit of about 5% by volume a taper waist of about 10 times longer is required (~300mm). For a stronger absorber ie. $\alpha >> 900m^{-1}$ the taper waist lengths required are proportionally shorter.

3.6 Thin Clad Fibres

3.6.1 Introduction

As dealt with above for fibre tapers the aim of enhanced probe sensitivity is achieved by maximising the evanescent field penetration into the chemical species to be sensed. A further method of increasing the evanescent field interaction power is by reducing the cladding thickness. Leaving enough cladding for total internal reflection to occur, but thin enough so that the evanescent wave associated with the propagating modes penetrates outside the cladding and interacts with the chemical resulting in absorption at the relevant wavelengths.

Figure 3.9 Thin clad fibre

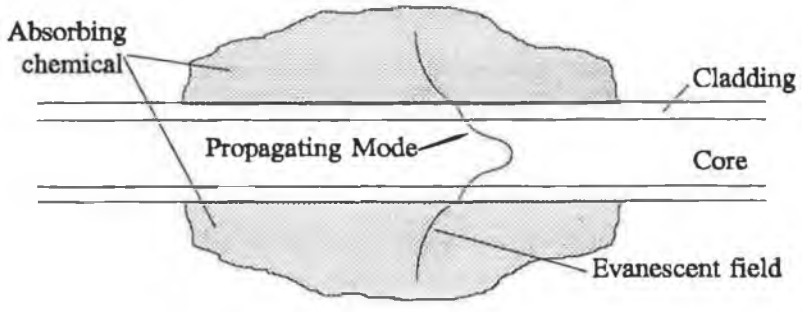

Thus by comparing thin clad fibres with fibre tapers an expression for the enhanced sensitivity that occurs with tapering can be achieved.

3.6.2 Experimental Setup

The thin clad fibre used was a 40/48μm zirconium fluoride fibre which due to the inherent brittleness of this material was supported on a perspex slab base. Due to the inflexibility of the support modifications had to be made to our launch/collection system detailed in section 2.3.2. The xyz fibre chuck positioner was removed from the launch system and replaced by a conventional xyz micro positioner with the thin clad fibre slab attached. Using this method the thin clad fibre was positioned until the maximum optical power in the desired region was achieved ie. 2500cm^{-1} to 4000cm^{-1}. A 300/340μm teflon clad fibre was butt coupled to the thin clad fibre to collect the transmitted light. This light was then collected from the 300/340μm teflon clad fibre using the normal collection system as in section 2.3.2.

Figure 3.10 Thin clad fibre experimental setup

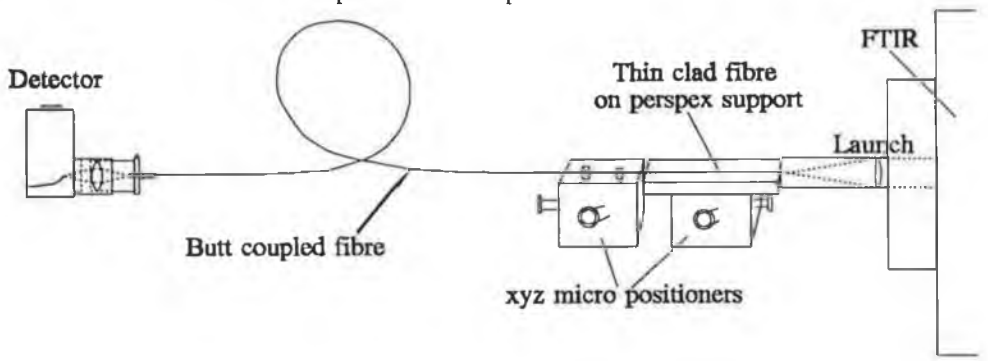

With the experimental setup as shown in Figure 3.10 a reference spectrum was taken at 16cm^{-1} resolution for 2000 scans in air. The thin clad fibre was then covered in 100% isopropylalcohol (C_3H_6OH) and a transmittance spectrum was taken. Using the Bomem software the two spectra were ratioed to give the transmission spectra as shown in Figure 3.11.

3.6.3 Theoretical and Experimental Analysis

Figure 3.11 100% isopropylalcohol spectrum using thin clad fibre

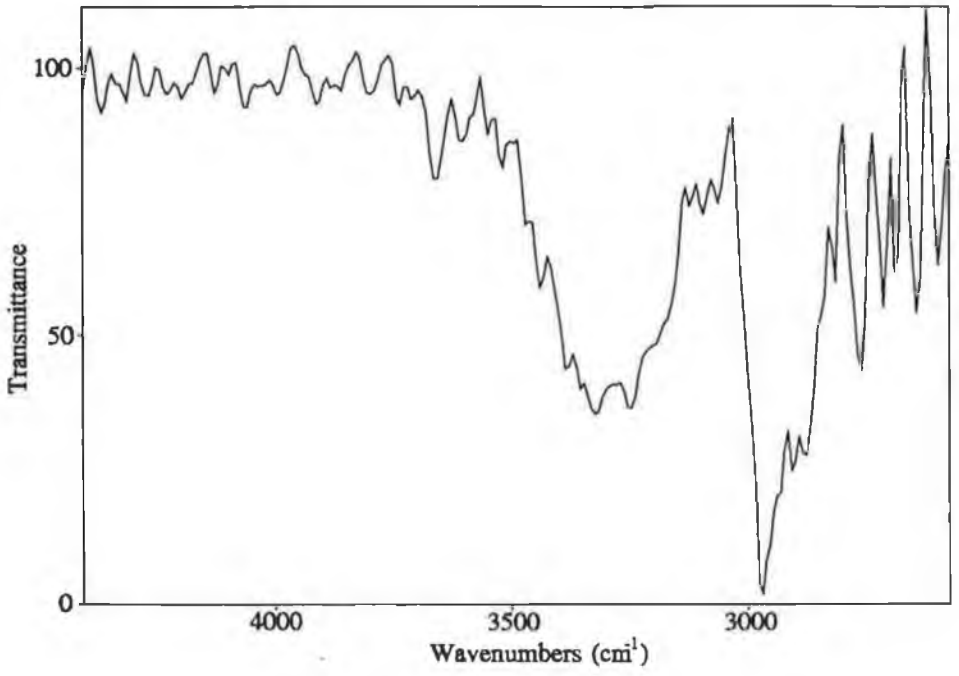

Thin clad fibres as shown have the sensitivity for sensing liquids, limited by noise due to low transmitted power levels. Thus the lowest concentration detectable

is 10% (assuming twice the noise value). Thus to detect gas to the same accuracy and neglecting the attenuation due to the fibre, a fibre length of 10m would be needed due to it being approximately 100 times easier to sense gases as mentioned before. In reality the fibre attenuation would make it impossible to sense gas using such a method.

With a transmittance of ~3% the fraction of power outside the cladding f^* can be estimated using a bulk absorption coefficient α - Erley and Blake (1965) - for isopropylalcohol at 3.3μm of 850m^{-1} and a sensing length L of 0.1m using

$$T = e^{-f^* \alpha L} \qquad \text{Eqn 3.10}$$

$$\Rightarrow f^* = \frac{3.506}{850\ (0.1)} \approx 0.041$$

assuming the NA of the fibre is filled.

A rough theoretical calculation of the power outside the cladding f^* may be derived from the evanescent power density term of Ruddy and Lardner (1993a) of

$$P(R) = \frac{P}{\pi a^2 R} e^{-2V(R-1)} \qquad \text{Eqn 3.11}$$

where P is the total power and R the normalised radius $R = r/a$.

Figure 3.12 Thin clad fibre mathematical schematic

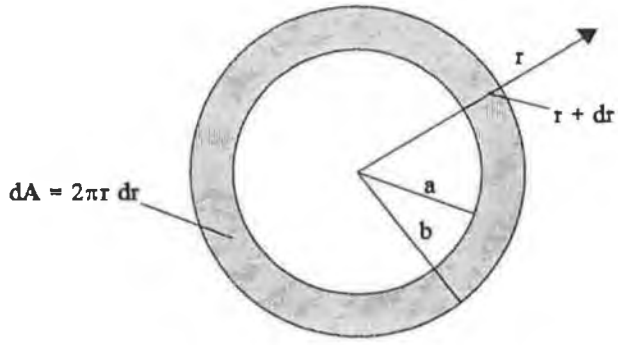

Integrating $P(R)\ 2\pi r\ dr$ over the zone $r = b$ to $r = \infty$ yields a power fraction f^* of

$$f^*(r>b) = \frac{e^{-2V(b/a-1)}}{V} \qquad \text{Eqn 3.12}$$

Taking a = 20μm, NA = 0.125, λ = 3.3μm yields a fibre V number of 4.76 and a power factor outside the cladding f^* for b > 24μm of 3.1%. This is quite close to the experimental value of 4.1%. In this theoretical analysis the cladding is assumed to be of index n_2 over the zone $r = a$ to $r = \infty$ unlike the actual situation where there is an interface between the glass cladding and the liquid sample at a radius b = 24μm.

3.7 Conclusions

The tapering of fibres and the use of thin clad fibres as a technique for drawing appreciable optical power into the sensing zone outside the fibre core is discussed. The experimental detection sensitivity for gas detection is compared with simplified models and found to correlate quite well.

The predicted sensor length to sense propane gas at its lower explosion limit of 5% was found to be a 0.33m taper waist and greater than 10m of thin clad fibre, when used in conjunction with the FTIR system. Thus for efficient gas sensing with fibre taper probes further manipulation would have to be done to enhance again the evanescent field in the taper waist region. The use of porous claddings and in particular a localised sol-gel overlayer in the waist region would achieve higher sensitivities as shown in chapter 2.

CHAPTER 4

Chapter 4

Special capillary Fibre Probes

4.1 Introduction

A fibre probe specifically designed for gas detection (using MIR evanescent wave attenuation) in conjunction with an FTIR spectrometer is evaluated for sensitivity and speed of response.

4.2 Design Considerations

As already stated the local numerical aperture $(n_1^2 - n_2^2)^{1/2}$ of an evanescent wave fibre probe determines the sensitivity of it for sensing purposes. If the lead-in fibre to the sensing region has a small numerical aperture (ie. a small range of possible bound mode angles) and the sensing zone has a large ***NA*** then the launched highest order modes are no longer high order when they reach the sensing region and as a result the probe sensitivity is low. This problem may be overcome by having the fibre core unclad over all its length, in which case if the input acceptance cone is filled (ie. if the light from the FTIR source fills the ***NA*** of the unclad fibre) then the rays striking the interface at the sensing region will include some which are incident at angles close to the local critical angle

$$\theta_c = Sin^{-1}\left(\frac{n_{chem}}{n_1}\right) \qquad \text{Eqn 4.1}$$

Where n_{chem} is the refractive index of the chemical being sensed

n_1 is the refractive index of the core glass.

This feature was designed into a fibre probe constructed by "Le Verre Fluore" in '92 and shown in Figure 4.1.

It consists of

i) a core of Zirconium Fluoride glass of 100μm diameter.

ii) a capillary of inner diameter 400μm and outer diameter 500μm which touches the core and is fused to it along one axis only. The capillary or partial cladding is of a lower refractive index glass than the core.

Figure 4.1 Capillary fibre probe cross-section

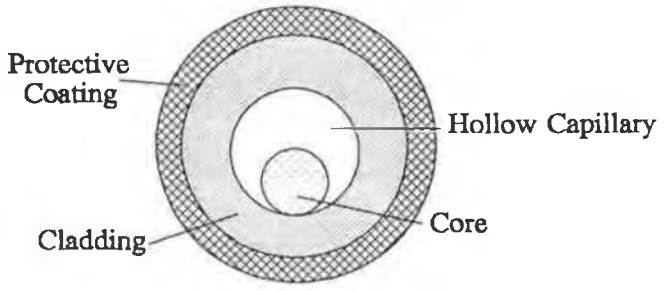

iii) a protective coating of 50μm thick polyacrylate.

The unit is sealed at each end ie. the hollow capillary is sealed with a glue at each end. Entrance and exit gas ports are incorporated into each end of the fibre being connected to the capillary cavity by two holes of approximately 100μm diameter, making the total fibre length the sensing region for the probe. Assuming laminar flow within the capillary probe and a coefficient of viscosity of $1x10^{-5}$ Ns/m^2 (methane gas has a viscosity of $1.08x10^{-5}$ Ns/m^2 according to Sears (1959)) the flow rate for a differential pressure of 0.5 bar (approximately $3.5x10^3$ N/m^2) can be calculated (from Poiseuilles Eqn) to be approximately $2x10^{-8}$m^3/s. This leads to a filling time for the sensor designed for methane at 0.5 bar gauge pressure to be about 10 seconds. This was considered to be a reasonable response time for a sensor probe.

Figure 4.2 Capillary probe

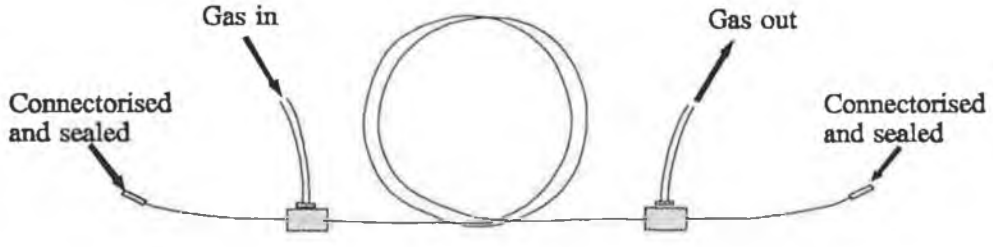

Since Zirconium Fluoride fibre has a refractive index approximately 1.52 to 1.47 over the range 0.4 to 5μm according to Mitachi (1989) and assuming a totally unclad 100μm diameter core fibre (NA = 1) theoretically this gives a V number of about $350/\lambda$ where λ is the wavelength of the light expressed in μm, or about 100 at a wavelength of 3.3μm at which many hydrocarbons absorb. The equivalent length

of the sensor is then

$$L_{eqv} = rL = \frac{4L\sqrt{2}}{3V} = 0.019L \qquad \text{Eqn 4.2}$$

where L is the actual length of the special capillary probe. With a length of 5.6m the equivalent length L_{eqv} for the direct transmission (rather than evanescent) spectroscopy is therefore 0.1m or 100mm. With attenuation coefficients α for Hydrocarbon gases having values of the order of $500m^{-1}$ (Ruddy (1993a) tabulates in Table 1 published values for various gases) transmission values of 60% giving absorption of 40% of the light are predicted for the hydrocarbon gases at 1% concentration if the probes numerical aperture is filled where the light enters the fibre from the FTIR. Thus with the design discussed above it was felt that the probe would have the necessary sensitivity and response time for sensing purposes of hydrocarbon gases at their lower explosive limits typically 5-10% - Lewis and Van Elbe (1951).

4.3 Experimental Setup

Due to the fact that the numerical aperture of the capillary fibre probe was greater than the effective launch numerical aperture of 0.125 as used previously and detailed in section 2.3.2 it was decided to use the high *NA* reflecting objective optical launch system shown in Figure 4.3. This was used in conjunction with two CaF_2 lenses (one concave and one convex) to produce a narrow 7mm beam which was then refocused by the reflective objective.

Figure 4.3 Reflective objective launch schematic

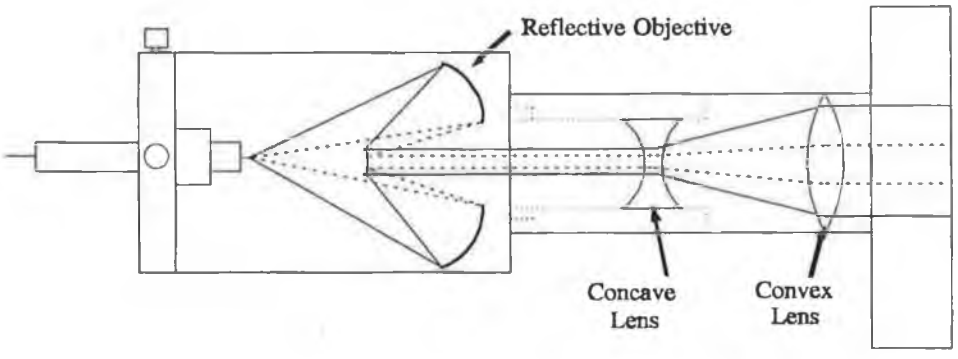

The light was launched into the special capillary fibre using this method and

collected using the normal lens configuration as in section 2.3.2. Using the reflective objective gave a higher ***NA*** launch but due to its configuration 17.5% of the central area was obstructed. These lower angles contribute to the low order propagation modes within the fibre and as such do not contribute largely to the sensing mechanism. Thus it was decided that using the high ***NA*** reflective objective would give us considerably more sensitivity than the lens launching system.

The special capillary fibre was aligned in the system as in Figure 4.4. Initially nitrogen (N_2) gas was inserted into the capillary under pressure and a reference spectrum taken at $8cm^{-1}$ resolution and 1000 scans. Then 100% methane was injected into the capillary and a similar transmission scan was done. This gave the transmission spectrum shown in Figure 4.6. The sensitivity using the large ***NA*** (0.28) launch was very much smaller than the predicted value. It was then decided to experimentally analyse the ***NA*** of the special capillary fibre for this reason.

4.4 Effective Numerical Aperture Measurement

Measurements of the effective numerical aperture of the probe were made using the method of plane wave launching into the fibre at various angles while the output fibre remains in a constant position in relation to the detector.

Figure 4.4 Experimental setup for numerical aperture measurement

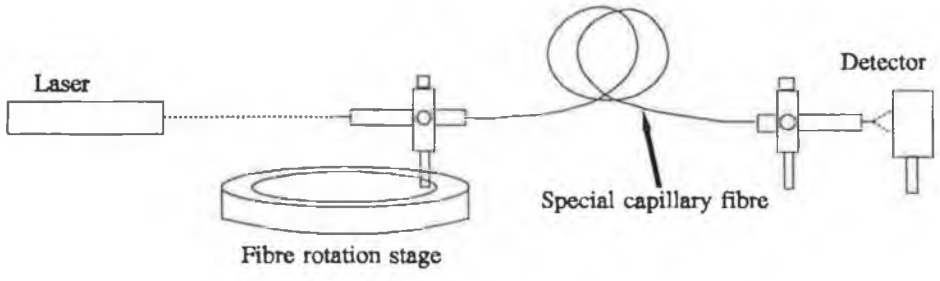

The fibre was placed exactly at the centre of rotation of the rotation stage and the laser was focused on the fibre end. This ensured that on rotation of the fibre launch stage all parameters remained constant except for the launch angle of the plane wave from the laser. The intensity of light launched in relation to launch angle θ was tabulated while keeping the detector and fibre alignment constant. This data was then

used to plot the graph of Intensity versus Sin(θ) shown in Figure 4.5 from which the *NA* of the special capillary fibre was calculated using the 5% power points.

Figure 4.5 Intensity versus Sin(θ) for the special capillary fibre probe

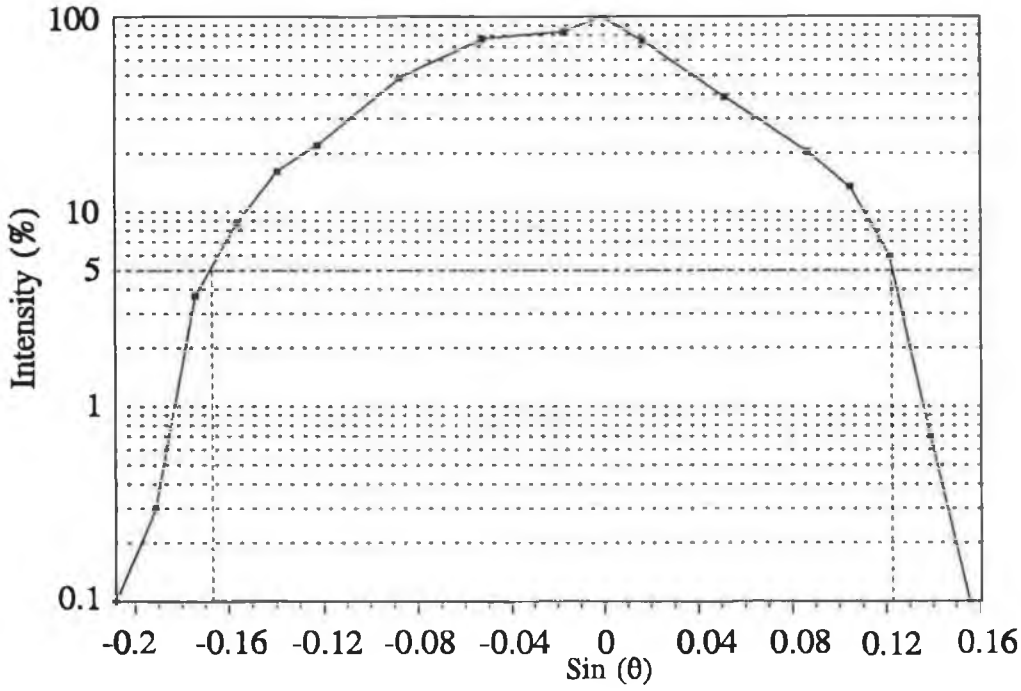

The *NA* of the connectorised special capillary fibre was calculated from the graph to be 0.145. This led to a large reduction in sensitivity as the fraction of optical power outside the core scales directly with *NA*, giving a reduced value of L_{eqv} determined by the ratio of NA_{theor}/NA_{exp}. Thus from the initial assumption of an effectively air clad fibre giving an *NA* of 1.0 to the experimental value of 0.145 causes the equivalent length L_{eqv} for direct transmission spectroscopy to go from $0.019L$ to $0.0028L$ or from 0.1m to 0.015m. With this experimental value for the *NA* of the special capillary fibre the predicted absorption for 1% methane is decreased from 40% to 7%. assuming a totally air cladding which the *NA* experiment proves to be unrealistic.

An *NA* measurement of the special capillary fibre was done with an unconnectorised section of fibre and the *NA* was found to be 0.185 which is 0.04 higher than the *NA* measured for the connectorised section of fibre. This leads us to believe that the main reason for the low *NA* of the fibre is due to the core capillary

interface acting as a core cladding interface to restrict the higher order modes or rays from propagating. This is possibly due to the interface not being consistently on a single axis of propagation[1].

4.5 Results and Analysis

The experimentally achieved absorption for 100% methane using the special capillary fibre was approximately 8% shown in Figure 4.6. This in contrast with the theoretical prediction of 7% absorption for 1% methane using the experimental *NA* value of 0.145 shows that the theoretical assumptions made were not valid for this fibre configuration used.

Figure 4.6 100% methane spectrum using the special capillary fibre probe

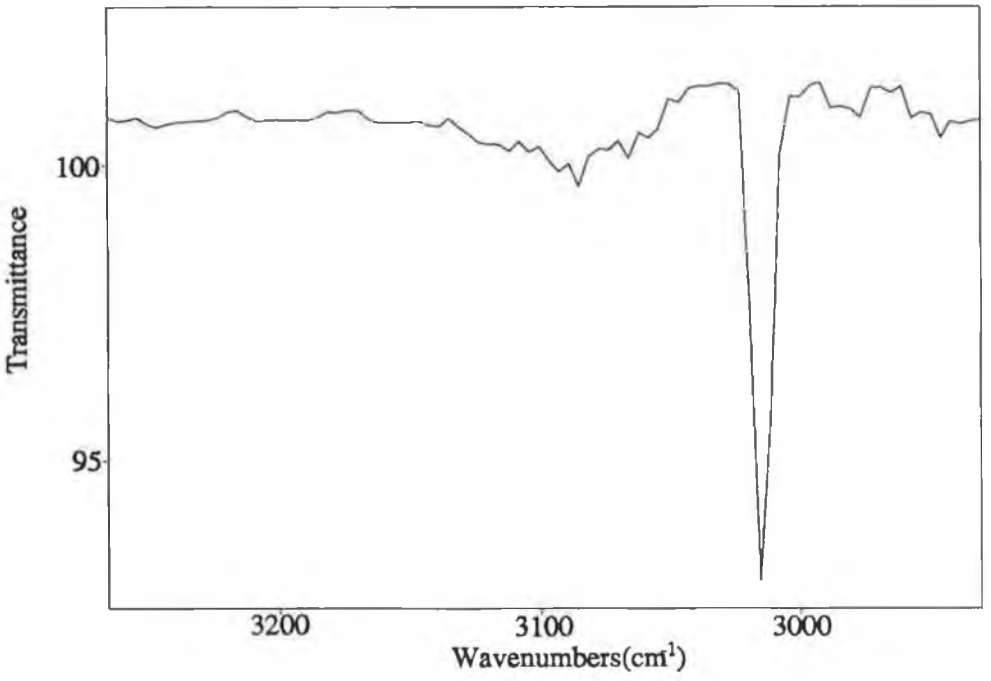

The assumption of a core only fibre was used in the calculation of the fractional power *f* outside of the cladding. This assumption was shown to be incorrect by the experimental value of the *NA* achieved. Unfortunately the fibre configuration is asymmetric and as such is extremely difficult to analyse theoretically. Thus instead of using a different theoretical approach we must readjust our figures by changing the

[1]The interface spirals down the fibre relative to the fibre mode propagation vector

fraction of power outside the core f by the ratio of the experimental NA over the initial theoretical NA. This method would give us an accurate value for sensitivity of a core only fibre with a launch NA of 0.145, but takes no account of the high refractive index difference between the core and the gas being sensed, which perturbs the propagating modes and causing the modes to propagate with their power shifted more into the capillary or effective cladding. Thus the fraction of power outside the core or cladding is dramatically reduced, causing the sensitivity of the special capillary fibre to be insufficient to sense gases to the required low level of concentration.

Though the fibre probe did not achieve the estimated sensitivity, it was shown to be a rugged design which overcame some of the problems of core only fibres and achieved a certain amount of gas sensitivity. The experimental absorption of 8% or 92% transmission using Beer's Law gives an equivalent length L_{eqv} for a gas transmission cell of 0.00017m.

4.6 Conclusions

The design of special capillary type fibre sensor probes is discussed. Sensitivity with one such device for gas detection is found to be low; this is explained in terms of a very low fibre numerical aperture due to light leakage at the fibre core/support substrate interface.

The low numerical aperture NA of the device and the shifting of the propagating modes into the support substrate and away from the core/air interface, which is the interactive region for this particular design caused the low sensitivity. This resulted in an absorption of 9% for 100% propane and a sensor length of 5.6m. When compared with the 25% absorption achieved with the teflon clad fibre for a sensor length of 0.33m, it shows that the sensitivity is quite poor, but the sensor design does give an immediate response to a change in the gas sample.

CHAPTER 5

Chapter 5
Gas Transmission Cells

5.1 Introduction

The detection of gases with small absorption coefficients using evanescent wave techniques is difficult due to the small fractional optical powers in the evanescent wave fields as already described. In this chapter measurements made on a fibre fed gas transmission cell are discussed with particular emphasis on flue gas analysis with respect to environmental gas emission control in industry.

5.2 Flue Gas Analysis

The products of combustion namely water vapour, carbon dioxide and carbon monoxide have absorption bands in the mid IR as do some of the products of impure fuels such as sulphur dioxide and various oxides of nitrogen. Listed in Table 5.1 are analytic wavelengths for various gases whose emission it is necessary to control for environmental reasons. Also estimates of their attenuation coefficients determined for the most part at $1cm^{-1}$ resolution are given.

Table 5.1 Bulk absorption coefficients[1] for flue gases

Gas	Analytic Wavelength μm	Wavenumber cm^{-1}	Bulk Absorption Coefficient m^{-1}
Carbon Dioxide	4.3	2326	750
Carbon Monoxide	4.6	2174	90
Nitrous Oxide	4.5 2.9	2222 3484	1130 55
Nitrogen Dioxide	6.2	1613	3000
Nitrogen Pentoxide	8.0	1248	4000
Nitric Oxide	5.3	1887	300
Sulphur Dioxide	8.6	1163	90

Typically flue gas compositions are listed in Table 5.2.

[1]Based on measurements by Erley and Blake (1965).

Table 5.2 Typical flue gas concentrations[2] present in a standard flue exhaust

Gas	Concentration
Carbon Dioxide	12-18% (0.12 to 0.18)
Carbon Monoxide	0-200 ppm (0 to $2x10^{-4}$)
Nitrous Oxide	100-700 ppm (1 to $7x10^{-4}$)
Nitrogen Dioxide	0-100 ppm (0 to $1x10^{-4}$)
Sulphur Dioxide	0-3000 ppm (0 to $3x10^{-3}$)

Thus to detect these gases at suitable concentration levels the relevant figures from Tables 5.1 and 5.2 can be used to establish the optimum gas transmission cell length. As the absorbance of a transmission cell of length L containing a gas of concentration c and absorption α is

$$A = \frac{c \alpha L}{2.303} \qquad \text{Eqn 5.1}$$

we can determine the minimum detectable "concentration length" product cL if we assume a minimum detectable absorbance value A_{min}, is

$$(cL)_{min} = \frac{2.303}{\alpha} A_{min} \qquad \text{Eqn 5.2}$$

The value of A_{min} will depend on the following parameters

i) the stability of the FTIR source

ii) the noise figure of the FTIR detector at the wavelength of interest

iii) the integration time used to make a single measurement.

These parameters determine the noise in the baseline of the transmission spectrum and thus the minimum detectable absorption, normally taken as twice the noise figure.

Taking an A_{min} value of 0.02 (corresponding to a 5% reduction in signal due to absorption or a 95% transmittance) we can predict the following $(cL)_{min}$ values for the gases listed in Tables 5.1 and 5.2 and the minimum detectable concentration values if

[2]These values depended on fuel type and are taken from "The theory of Combustion", Dearborn Chemicals Ltd.

a) the transmission path length is 0.75m

b) the minimum detectable transmission power reduction is 5%
ie (A_{min}=0.002)

Table 5.3 $(cL)_{min}$ values for standard flue exhaust gases

Gas	$(cL)_{min}$ value m^{-1}	C_{min} values in ppm
Carbon Dioxide	~$6x10^{-5}$	~80
Carbon Monoxide	~$5x10^{-4}$	~680
Nitrous Oxide	~$4x10^{-5}$	~53
Nitrogen Dioxide	~$1.5x10^{-5}$	~20
Nitrogen Pentoxide	~$1x10^{-5}$	~15
Nitric Oxide	~$1.4x10^{-4}$	~200
Sulphur Dioxide	~$5x10^{-4}$	~680

Comparison of the predictions of Table 5.3 and the typical flue gas composition concentrations of Table 5.2 indicate that a 0.75m path length is expected to be sufficient to detect carbon dioxide and nitrous oxide at their likely flue gas concentrations and only high concentrations of sulphur and nitrogen dioxide but not any of the other gases. For these a longer transmission cell is required.

It should be pointed out that the values of the absorption coefficient α used in Eqns 5.1 and 5.2 were the room temperature values. With stack temperatures of the range 90-500°C the Doppler Effect will result in line broadening and a corresponding reduction in the value of α. This in turn will lead to an increase in either the minimum detectable concentration of a gas or the transmission path length required to observe a certain reduction in optical power due to attenuation.

This fact can be taken into account when calibrating an actual working system, a table of α values for varying temperature can be used to calculate the percentage of each gas present.

5.3 Design of the Gas Transmission Cell

A gas transmission cell of path length 0.75m was designed at Culham Laboratories UK for flue gas analysis in conjunction with an FTIR. The specific parameters of the FTIR as used in the design are detailed in section 1.5. The optical power is brought to and from the cell by a 200μm core multimode step index IR transmitting fibre of zirconium fluoride. The initial launch/collection system used to transmit the light to and from the FTIR is the basic simple lens setup as shown in section 2.3.2. The light coupling from the input fibre to the gas transmission cell and then from the transmission cell back into the collection fibre was via matched parabolic mirrors as shown in Figure 5.1.

Figure 5.1 Experimental setup for the gas cell probe

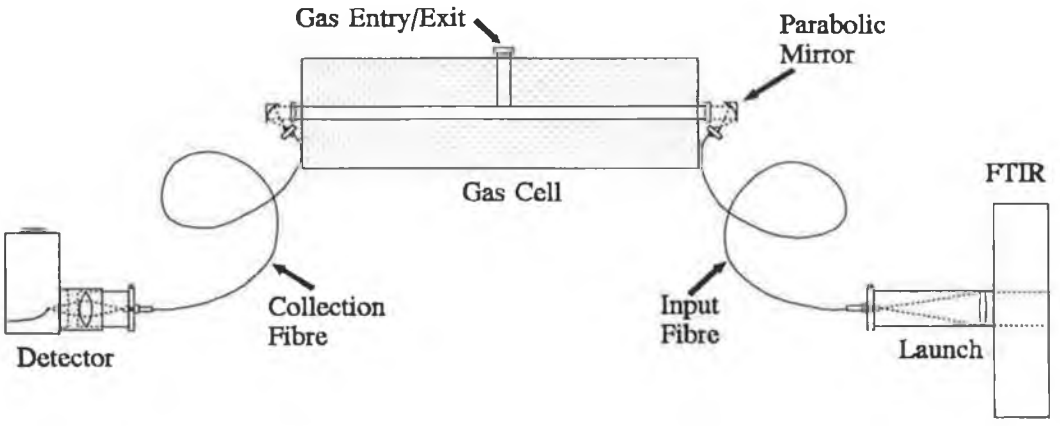

The parabolic mirrors were custom designed to couple the optical power from the FTIR source to the transmission cell via the IR transmitting fibre (NA = 0.2) as shown and to redirect the transmitted cell beam into the fibre which carries it to the detector of the FTIR. To maximise the efficiency of the transmission cell system the Newport fibre positioners to and from the transmission cell have the standard three (xyz) directions of movement as well as rotation in the xz-plane ie. parallel to the optical bench. Thus the total system can be seen to have four areas of alignment, two for each fibre and a total of fourteen variables when aligning the total system. This leads to tedious and time consuming process when aligning the system. This system was considered necessary to provide the necessary flexibility in the lab based gas transmission cell. In an industrial arrangement, the optics could be aligned initially

and then permanently cemented in place to ensure uniform alignment over all transmission spectra.

The system also consisted of a single entry/exit gas control system. Thus by using a vacuum pump to evacuate the system and gas valves to release the relevant gases into the system, a very efficient and accurate means of inserting the sample gases was achieved. This method was preferred over the simpler double entry/exit method as only small sample bottles of the relevant gases were available, and it gave greater control over the dispersion of these dangerous gases into the environment.

Not shown in Figure 5.1 but included in the transmission cell unit was a PID temperature controlled electric heater element, which was used to simulate typical flue gas temperatures. The system had an operating range of between room temperature approximately 20°C and 325°C and was calibrated so that any temperature in this range could be achieved.

5.4 Experimental Setup and Results

The operation of the system was checked using a sample of 0.5% methane. The experimental setup as mentioned above was aligned using a Helium Neon laser to initially roughly align the gas transmission cell input and collection fibres. When the full system was completely aligned a reference was taken with 100% Nitrogen (N_2) present in the transmission cell, placed by means of the single entry/exit gas port in conjunction with the vacuum system. The reference was taken at $1cm^{-1}$ resolution and was done for 1000 scans. The system was then evacuated and the 0.5% methane and the 99.5% nitrogen sample was placed in the transmission cell and a transmission spectrum taken. This was also done at $1cm^{-1}$ resolution and 1000 scans.

A transmittance of 3% (ie 97% absorption) was observed at the 3.32μm analytic wavelength which is consistent with an absorption coefficient α of $1001m^{-1}$. Hanst (1975) quotes a value for methane of $1200m^{-1}$. The deviation of the measured and quoted value may be attributed to the accuracy of the transmittance value or the 0.5% concentration value of the gas. The variation in the absorption coefficient α

Figure 5.2 0.5% Methane spectrum using the gas transmission cell

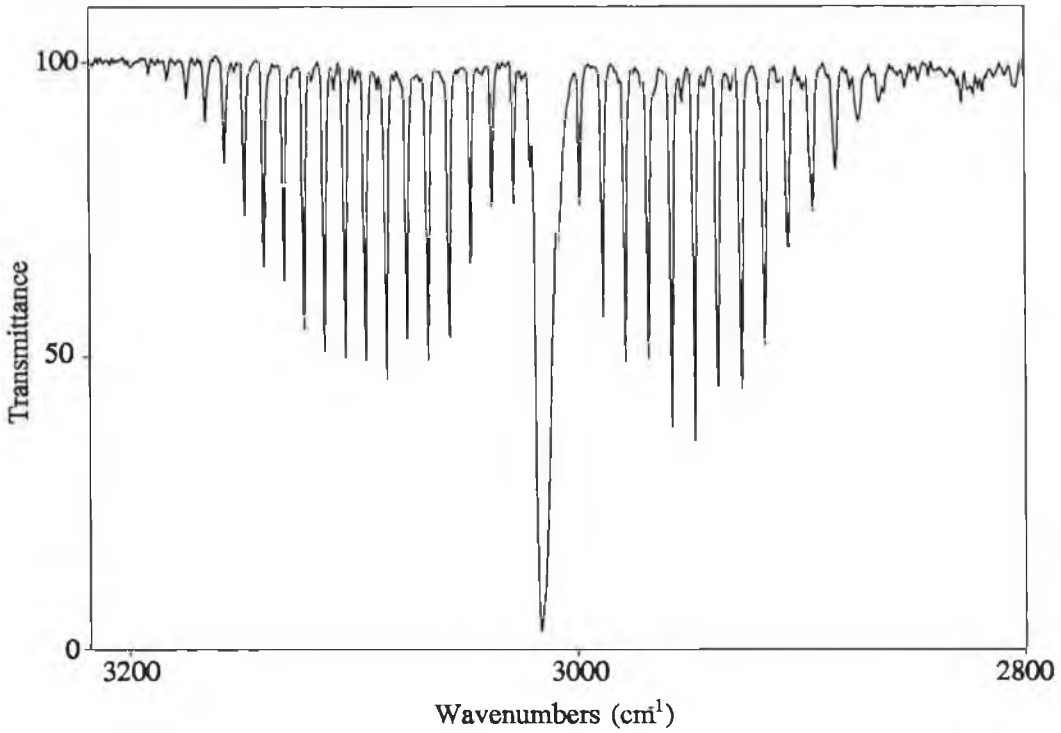

from $1001m^{-1}$ to $1200m^{-1}$ corresponds to a change in transmittance from 3% to 1.5% and in concentration from 0.5% to 0.42% methane, both of which could easily be the case as they are well within the margin of error associated with the spectrum due to noise (~1.5%) - see Figure 5.2 and the unknown accuracy of the mass flow controllers when controlling the regulated gases into a gas chamber under vacuum.

With the FTIR set to a resolution of $1cm^{-1}$ spectra of the two flue gas samples provided by Culham Laboratories with the concentrations listed in Tables 5.4 and 5.5 were taken. These were provided by Culham Laboratories to test the sensitivity of the total system with regard to the levels of pollutants needed to be sensed for a satisfactory flue gas monitoring system. The transmission spectra were referenced with respect to the transmission spectrum of the vessel system filled with Nitrogen (N_2). In both cases the spectra were taken using 1000 scans co-added and at a resolution of $1cm^{-1}$.

Table 5.4 Gas concentrations for sample #1

Gas	Pressure	Concentration
Carbon Dioxide	2.5 bar	12.2% or 122,000 ppm
Sulphur Dioxide	1.0 torr	64 ppm
Nitrous Oxide	1.5 torr	96 ppm
Nitrogen	18 bar	~87%

1 bar = 760 torr

On examination of Figure 5.3 the transmission spectrum of gas sample #1 at various temperatures, strong absorption structure is observed at around 3700cm^{-1} or 2.7μm and 2300cm^{-1} or 4.35μm which is due to carbon dioxide which has strong vibration and rotation bands in these regions. The smaller absorption peak around 5000cm^{-1} or 2.0μm is also due to carbon dioxide. The structure at 3800cm^{-1} or 2.63μm is possibly due to water vapour.

Figure 5.3 Spectra of gas sample #1 at 20°C (top) and 325°C (lower)

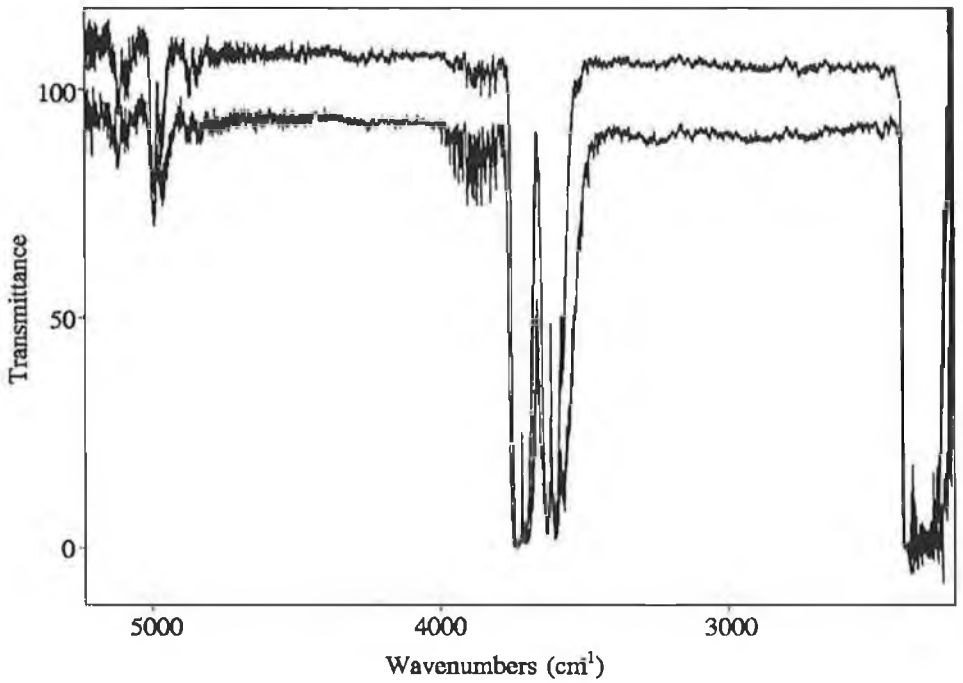

The structure visible at around 2300cm^{-1} is the very strong absorption band of CO_2 and it is the main CO_2 peak in the region analysed. With a bulk absorption coefficient of 750 m^{-1} (Table 5.1) and a concentration of 0.122 for CO_2 (Table 5.4)

the predicted transmittance for a 0.75m path length is effectively zero ($< 1x10^{-20}$). The saturation absorption observed is consistent with this.

The presence of SO_2 (at 64 ppm) is not observed; there is no visible structure at 2500cm^{-1} (the $\upsilon_1 + \upsilon_3$ structure) OPERA (1993) quotes an absorption coefficient of $5x10^{-7}$ $cm^{-1}ppm^{-1}$, which predicts a transmittance of 99.77%. As can be seen from Figure 5.3 the baseline noise would mask completely such a small effect (0.23% absorption). Similarly the presence of NO (at 96 ppm) is not observed; there is visible structure at 3750cm^{-1} (the 2υ structure). An absorption coefficient of $1x10^{-7}$ $cm^{-1}ppm^{-1}$ quoted by OPERA (1993) predicts a transmission of 99.92%. Thus similar to the SO_2 structure, the NO structure is lost in the baseline noise. The NO is also masked by the CO_2 and water peaks around 3700cm^{-1}, which would make it extremely difficult to analyse quantitatively with CO_2 or water present in the gas sample, as both of these are present in any flue gas emissions an other absorbing frequency for NO would have to be used.

Table 5.5 Gas concentrations for sample #2

Gas	Pressure	Concentration
Carbon Dioxide	3.0 bar	18.8% or 187,000 ppm
Carbon Monoxide	1.5 torr	104 ppm
Sulphur Dioxide	1.0 torr	69 ppm
Nitrogen	16 bar	~80%

1 barr = 760 torr

Turning now to sample #2, whose spectrum is shown in Figure 5.4 the CO_2 bands are again visible and SO_2 does not appear as detailed for sample #1. The Carbon monoxide present is predicted to give a transmission of 99.3%, this effect would have been lost in the baseline noise, but the system cut off due to the permanent noise reduction filter installed in the detector is above the carbon monoxide absorption at 2174 cm^{-1} or 4.6μm.

Figure 5.4 Spectra of gas sample #2 at 20°C (top) and 325°C (lower)

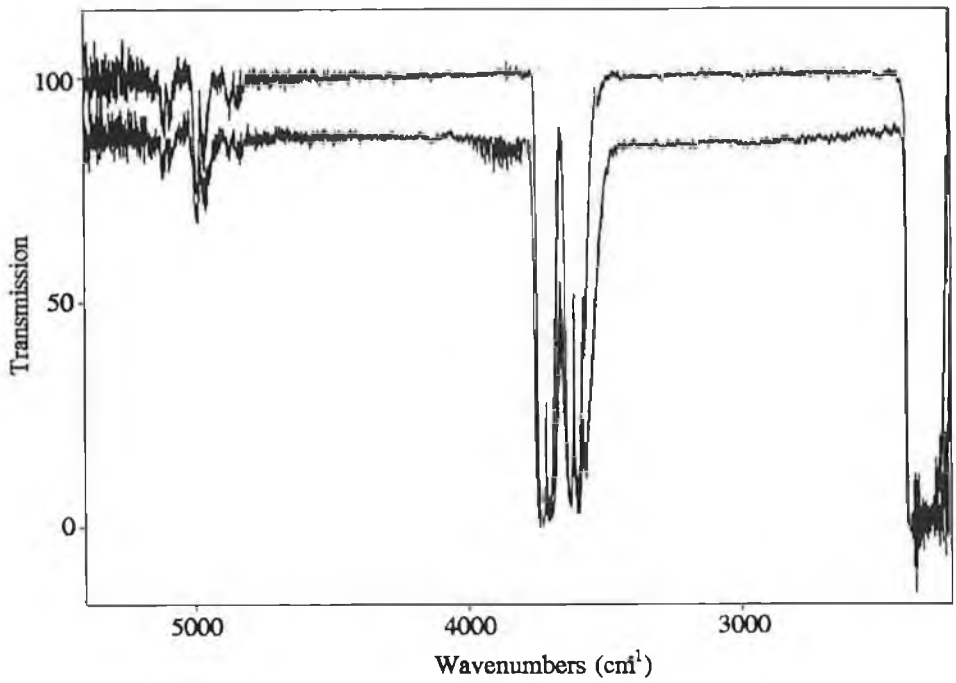

The spectra shown in both Figures 5.3 and 5.4 show a distinct variation between spectra taken for the same sample but at different temperatures. The top spectra in both cases is done at room temperature (20°C) and the lower spectra at 325°C, the maximum temperature allowed with the experimental system. This reduction with increased temperature may be due to fractional changes in alignment of the system optics as the gas chamber expanded with temperature. This was demonstrated by recording spectra for the various temperatures with a totally evacuated gas chamber. The results showed an equivalent reduction of power throughput with temperature. Thus in an industrial gas chamber the reference spectrum could be taken at the expected transmission temperature and the optics permanently aligned to prevent any misalignment due to small variations in the flue operating temperature.

The gas chamber was sealed after each sample gas was injected, this was done to prevent any contamination. Thus as the temperature was increased the pressure increased according to the ideal gas law. The increased pressure due to temperature

resulted in pressure broadening of the line width - see Figures 5.3 and 5.4.

5.5 Conclusion

The detection of flue gas constituents using an FTIR fibre coupled to a 0.75m transmission cell is limited to the strong absorber Carbon Dioxide and none of the Nitrogen or Sulphur Oxides important as environmental pollutants can be seen. These results agree with the expected theoretical values and it must be assumed that Culham Laboratories used a 0.75m path length for the transmission cell to imitate an actual flue diameter for which the system was designed.

In general flue diameters are typically of the order of meters, thus in this case a fibre fed transmission flue measurement where the flue itself acts as the transmission cell or a sizeable fraction of it used for this purpose, would provide a substantially larger optical path length and a corresponding increase in absorbance. It would appear that the sensitivity of such a system would be too low to detect the pollutant gases at their typical concentrations. Such an open path system cell would suffer from signal reduction due to soot depositing on the optical components. An aspirator drawing off flue gases through a fine mesh filter would overcome this problem but the need for substantial path lengths of several meters still remains.

Thus the use of a multi path gas transmission cell in conjunction with an aspirator would seem to offer the best option for the sensitivity necessary to detect the low attenuation pollutant flue gases such as the sulphur and nitrogen oxides.

CHAPTER 6

Chapter 6
Conclusions and Possible Future Work

6.1 Overall Conclusion

This work investigated various fibre optic probes suitable for use with a fourier transform infrared spectrometer for the detection of fluids with absorption lines or bands in the near to mid infrared. Both evanescent wave and direct transmission spectroscopy techniques were used.

For the evanescent wave devices evaluated the importance of the cladding or overlayer refractive index was critical to the device sensitivity. The drawing out of the fibres optical power outside the core by designing the cladding or overlayer refractive index to be close to that of the fibre core glass was understandably of prime importance to the resolution that could be achieved by the device.

Of the various probe designs, porous cladding, sol-gel overlayers, tapers, thin clad fibres and special capillary fibres the porous cladding approach was found to be the most promising, with an absorption of 25% for 100% propane achieved with a sensing region of only 0.33m. It also offers the best possibilities for distributed sensing. The theoretical fractional power outside the core agreed quite well with the experimental value, once the lower resolution of our system was taken into account. The time needed for the gas to diffuse into the porous cladding was the only drawback to this method of evanescent gas sensing.

Tapers and sol-gel overlayers are suitable only for local sensing with the tapered fibres being very fragile. Also both the sol-gel overlayers and the fibre tapers are subject to contamination or residual traces of the gas being sampled which may leave a memory effect with the sensors (ie. the devices sensitivity will show hysteresis). Aside from these problems, both these methods provided an excellent means of enhancing the fractional power in the evanescent field of a given fibre. Thus these two methods are valuable tools in evanescent gas sensing, achieving an absorption of 9% using sol-gel overlayers on a polished block and 15% using a single

mode fibre taper for 100% propane. The sensitivity achieved for the sol-gel overlayers was greater than theoretically expected, while for tapers the theoretical and experimental results agreed extremely well.

The thin clad fibres were found to be insensitive to gases unless long lengths were used. Due to fact that liquids have a higher refractive index and higher attenuation coefficients, thin clad fibres were found to extremely sensitive in detecting liquids, achieving approximately 100% absorption for 100% isopropylalcohol with an active sensor length of 0.1m. The fractional power outside the fibre was found to be 4.1% experimentally and 3.1% theoretically, giving very good agreement for the simple model used.

The special capillary fibre was found to have lower sensitivity to gases than predicted. This, it is believed was due to the low numerical aperture of the design, caused by light leakage at the core/support structure interface and also the displacing of the propagating modes from the core centre towards the core/support interface, and away from the core/air interface which is the interactive region for this probe design. This resulted in a 9% absorption for 100% propane with an interactive sensor length of 5.6m. The sensitivity - though lower than expected - does giving an immediate response for a change in the sample gas.

The gas transmission cell proved to be the most sensitive means of gas detection, with 97% absorption for 0.5% methane. The gas transmission cell when used to analyse the two samples of typical flue gas mixtures, showed that a path length of 0.75m was not sufficient to sense flue emission gases at a low enough concentration. A path length of several meters would be needed for such accuracy with low attenuation flue emission gases. These experimental results agreed with the theoretical values when the calculations were done using typical flue gas concentrations and attenuation coefficients.

Due to the low refractive index of the gases (typically 1.0) evanescent wave spectroscopy of gases with high index glass fibres is particularly difficult due to the

confinement of the evanescent field. The brittleness and resulting problems of handling zirconium fluoride fibres makes their manufacture as gas sensors particulerly difficult; accordingly they are unsuitable for the rigours of the workplace.

Improvements in the attenuation coefficient and ruggedness of fluoride fibres, may eventually make them an industrial possibility, if not for gas then for liquid sensing.

6.2 Possibilities for Future Work

All the work done using infrared transmitting fibres for this thesis was with zirconium fluoride fibre. This is by no means the only infrared transmitting fibre available. The two most important alternatives to fluoride fibres are the chalcogenide and silver halide fibres which both have a far wider transmission band in the infrared. Typically they transmit from 0.5 to 20μm, thus providing far greater scope for identifying a wider variety of chemical types. The draw back to these types of fibres is that they have larger attenuation coefficients than fluoride fibres. Thus chalcogenide and silver halide offer good possibilities for similar work in these areas. Polymer clad fibres of cladding materials other than teflon could be examined.

With respect to the fibre probes analysed for this work, there are certain areas that could be pursued further. The sol-gels used in our experimental work were silicon based and as such were not ideally suited for work with fluoride fibres. The use of zirconium fluoride sol-gels, though not commercially available to date, but the subject of development, would be very beneficial to the sensitivity achieved. Also the pore size of the sol-gel overlayer could be increased, so as to reduce the diffusion time associated with sol-gels. Finally sol-gel cladded fibres and sol-gel coated tapered regions could increase the sensitivity previously achieved by utilising the porous nature of the sol-gel glass, without affecting the refractive index of the cladding.

Fibre fed transmission sample cells offer much higher detection sensitivity than evanescent wave sensors but in an industrial environment they would require "grab sampling" techniques to prevent the soot depositing on the optical components. The

use of a multi path gas transmission cell in conjunction with an aspirator to extract the gas samples through a fine mesh would overcome these problems. Care is required as this may cause modifications to the sample composition between the sampling point and the analysing system (the sample cell and FTIR spectrometer).

References

Abramowitz M. and Stegun I.A. "Handbook of mathematical functions", National Bureau of Standards Washington DC (1964).

Birks T.A. and Li Y.W. "The shape of fiber tapers", J. Lightwave Tech. (USA), Vol 10 (4), pp 432-438 (1992).

Bobb L.C., Shankar P.M. and Krumboltz H.D. "Bending effects in Biconically Tapered single mode fibres" IEEE J. Lightwave Tech., 8, pp 1084-1090 (1990).

Bomem, "FT-IR User's Guide, Michelson series", (1989).

Brighan E.O., "The Fast Fourier Transform", Prentice-Hall (1974).

Brandrup J. and Immergut E.H. (Eds.), "The Polymer Handbook", Wiley, New York (1979).

Carter S.F., Moore M.W., Szebesta D., Williams J.R., Ranson D. and France P.W. "Low loss fluoride fibre by reduced pressure casting", Electron. Lett. (UK) Vol. 26 (25), pp 2115-17 (1990).

Cochran W.T., Cooley J.W. et al, "What is the Fast Fourier Transform ?", Proceedings of the I.E.E.E. Vol. 55 (10), October (1967).

Curran J. "Optical fibre tapering furnace", Physics Project Dublin City University (1992).

De Grandpre M.D. and Burgess L.W. "A fibre optic FT-IR evanascent field absorbance sensor", Appl. Spectros. Vol 44, pp 273 (1990).

Dewynne J., Ockendon J.R. and Wilmoth P. "On a mathematical model for fibre

tapering", SIAM J. on Appl. Maths., 49, pp 983-900 (1989).

Driver R.D., Downing J.N. and Leskowitz G.M. "Evanescent wave spectroscopy down infrared transmitting optical fibres", S.P.I.E. Vol. 1591, Infrared Fibre Optics III, pp 168-179, Boston (1991).

Egalon C.O., Thesis "Injection efficiency of bound modes", William and Mary University, Virginia, USA. (1990).

Eisenmann M. and Weidel E. "Single mode fused biconical couplers for wavelength division multiplexing with channel spacing between 100 and 300nm", IEE J. Lightwave Tech. 6, pp 113-119 (1988).

Erley D.S. and Blake B.H., "Infrared Spectra of gases and vapours", Vol. II , The Dow Chemical Company, Michigan, USA. (1965).

Gloge D. "Weakly guiding fibres", Appl. Opt. 10, pp 2252-2258, (1971).

Hanst P.L., Spiller L.L., Watts D.M., Spence J.W. and Miller M.F. "Infrared measurement of fluorocarbons, carbon tetrachloride, carbonyl sulphide and other atmospheric trace gases", J. Air Pollut. Control. Assoc. 25 (12) pp 1220-1226 (1975).

Harrick NJ. "Internal Reflection Spectroscopy", Harrick Scientific Corp. NY, (1987).

Heo J., Rodrigues M., Saggese S. and Siegel G.H. Jr. "Remote fiber-optic chemical sensing using evanescent wave interactions in chalcogenide fibers", Appl. Opt. 30, pp 3944, (1991).

Katz M., Bornstein A., Schnitzer I. and Katzir A. "Evanescent wave spectroscopy using chalcogenide glass fiber: theoretical analysis and experimental", S.P.I.E. Vol. 1591, Infrared Fibre Optics III, pp 236-245, Boston (1991).

Krska R., Rosenberg E., Taga K. and Kellner R. "Polymer coated silver halide infrared fibers as sensing devices for chlorinated hydrocarbons in water", Appl. Phys. Lett. 61 (5), pp 1778-1780 (1992).

Kenny R.P., Birks T.A. and Oakley K.P. "Control of Optical Fibre Taper Shape" Electron. Lett. (UK), 27 (18), pp 1654-1656 (1991).

Lewis B. and Von Elbe G. "Combustion Flame and Explosions of Gases", Academic Press (1951).

Love J.D., Henry W.M., Stewart W.J., Black R.J. Lacroix S. and Gunthier F. "Tapered Single mode fibres and devices: Parts 1 and 2", IEE Proc. J. 138 (5), pp 343-354 (part 1), pp 355-364 (part 2) (1991).

Mac Craith B.D., Ruddy V. and M^{c}Cabe S. "The suitability of single-mode fluoride fibres for evanescent wave sensing", SPIE. Vol. 1587 (1991).

Mac Craith B.D., Ruddy V., Potter C., O'Kelly B. and M^{c}Gilp J.F. "Optical waveguide sensor using evanescent wave excitation of fluorescent dye in sol-gel glass", Elect. Letts. 27 (14), pp 1247-1248 (1991).

Margalit E., Dodiuk H., Kosower E.M. and Katzir A. "Infrared fibre evanescent wave spectroscopy for in-situ monitoring of chemical processes", Proc. S.P.I.E. 1048, pp233-240 (1989).

Mazé G., Cardin V., Chiquet F. and Poulain M. "Fluoride glass fiber-optic sensors: realizations and prospects", Springer Proc. in Physics, Vol. 44, pp 20-29 (1989).

M^{c}Cabe S., "Investigation of evanescent wave gas sensing using infrared transmitting optical fibres", Thesis submitted to: Dublin City University, (1993).

Messica A., Katzir A., Schiessl U. and Tacke M. "Liquid and gas fiber optic

evanescent wave spectroscopy by tunable laser", S.P.I.E. Vol. 1591, Infrared Fibre Optics III, pp 192-197, Boston (1991)

Mitachi S. "Dispersion measurement on fluoride glasses and fibre", J. Ligtw. Tech., 7 (8) pp 1258 (1989).

Muhammad F.A. and Steward G. "D shaped fibre design for methane gas sensing", Electron. Letts. 28 (13), pp 1205-1206 (1992).

OPERA, "Optical Probes for Emission Reduction and Analysis", Ref. CEC OPERA R/I, Contract No. STEP-CT90-0114 (DTEE), January (1993).

Pedrotti F.L. and Pedrotti L.S. "Introduction to Optics", Prentice-Hall Inc. NJ., pp 503-504 (1987).

Rabiner L.W. and Gold B., "Theory and application of digital signal processing", Prentice-Hall (1975).

Ruddy V. "An effective attenuation coefficient for evanescent wave spectroscopy using multimode fibre", Fibre and Integ. Optics 9, pp 142-150 (1990a).

Ruddy V. and Lardner K. "Porous clad Fibres as sensor probes", Int. J. Optoelectronics 8 (1), pp 87-95 (1993a).

Ruddy V. "Private Communication", (1993b).

Ruddy V., M^{c}Cabe S. and Mac Craith B.D. "Detection of propane by IR-ATR in a teflon clad fluoride glass optical fibre", Appl. Spectros. 44, pp 1461-1463 (1990b).

Saito M., Sato S. and Miyagi M. "Spectroscopic gas sensing with infrared hollow waveguides", S.P.I.E. OE/Fibers, Boston, pp 1796-1836 (1992).

Seers F.W. "An Introduction to Thermodynamics, The Kinetic Theory of Gases and Statistical Mechanics", Addison Wesley Publ. Corp. Inc. USA., Table 13-1 pp 266 (1959).

Snyder A.W. and Love J.D. "Optical Waveguide Theory", Chapman and Hall, NY (1983).

Tekippe V.J. "Passive fibre-optic components made by the fused biconical taper process", Fiber Integ. Opt., 9, pp 97-123 (1990).

Tseng S.M. and Chen C.L. "Side polished fibres", Appl. Opt. 31 (18), pp 3438-3447 (1992).

Van Etten W. and Van Der Plaats J.V. "Fundamentals of Optical Fiber Communications", Prentice Hall N.Y. (1991), Figure 1.9, pp 9.

Worrell C.A., Giles I.P. and Adatia N.A. "Remote gas sensing with mid infrared hollow waveguides", Electron. Letts. 28 (7), pp 615-616 (1992).

Yoshikawa H., Sugata A., Watanabe M. and Ohno Y. "Distributed fluid sensor using essentrically cladded fibres", Electron. Comm. in Japan 71 (2), pp 89-97 (1988).